International Journal of Coal Geology 191 (2018) 95–111

Contents lists available at ScienceDirect

International Journal of Coal Geology

journal homepage: www.elsevier.com/locate/coal

Role of water–rock interaction in the geochemical evolution of Marcellus Shale produced waters

Thai T. Phan[a,b,*,1], Amelia N. Paukert Vankeuren[a,c], J. Alexandra Hakala[a]

[a] National Energy Technology Laboratory, U.S. Department of Energy, Pittsburgh, PA 15236, United States
[b] Department of Geology and Environmental Science, University of Pittsburgh, Pittsburgh, PA 15260, United States
[c] Geology Department, California State University, Sacramento, Sacramento, CA 95819, United States

ARTICLE INFO

Keywords:
Produced water
Water-rock interaction
Marcellus Shale
Uranium
Carbonate dissolution
Lithium isotopes
Radiogenic strontium isotopes
Core flood experiments

ABSTRACT

Knowledge of geochemical processes that occur during hydraulic fracturing of shale resources for natural gas recovery can provide insight into in situ mineral precipitation and dissolution reactions that affect shale pore and fracture networks, and ultimately the ability to recover natural gas. Measurement of dissolved chemical species in produced waters, which serve as indicators of water-rock reactions in the reservoir, is one approach for monitoring subsurface geochemistry. However, an ability to distinguish effects of water-rock reactions versus reservoir fluid mixing on chemical concentration and speciation in produced waters requires experimental investigation to better understand natural geochemical tracer behavior.

In this study, we explored Li, Sr, and U as geochemical tracers of ion–exchange and mineral dissolution reactions occurring during a series of flow-through laboratory experiments designed to evaluate mineral reactions occurring in shale reacted with hydraulic fracturing fluid (HFF). The experiments, reported in detail in a separate study (Paukert Vankeuren et al., 2017), were designed to emulate shut-in conditions (period after hydraulic fracturing but before production when HFF remains in the reservoir to allow for opening of new fractures for hydrocarbon recovery) for Marcellus Shale undergoing hydraulic fracturing in southwestern Pennsylvania, USA. In the companion study presented here, effluent samples from the core flood experiments were analyzed for changes in Li isotopes (δ^7Li), radiogenic Sr isotopes (ε_{Sr}^{SW}), and U concentration as possible unique geochemical tracers to indicate water-rock reaction. Experimental and reactive transport modeling results demonstrated that the peak of U in experimental effluents is derived from dissolution of U-containing calcite, which may explain the pulse of U observed in produced water collected from hydraulically fractured Marcellus Shale on the first day of flowback. Experimental results also showed that changes in δ^7Li values and ε_{Sr}^{SW} from the flow-through experiments differ from values measured in a time series of produced waters from Marcellus Shale gas wells. Thus, although ion–exchange and mineral dissolution and precipitation reactions result in an observable change in Sr isotope signals in laboratory experiments, this change may not be identifiable in produced waters in the field due to complications associated with geologic heterogeneity and overprinting of other signals such as fluid mixing and transport. While U shows some promise as a tracer of HFF-shale reactions, particularly carbonate dissolution, it may be necessary to continue searching for other tracers present in produced waters to aid in elucidating in situ water-rock reactions of interest.

1. Introduction

Increasing extraction of natural gas from the Marcellus Shale in the eastern United States has motivated a wide range of research topics including characterization of reservoir properties to optimize production (e.g., Wilkins et al., 2014), and the study of environmental issues associated with upstream activities such as well pad development, drilling, hydraulic fracturing, and gas production (e.g., Brantley et al., 2014; Phan et al., 2015; Soeder et al., 2014). Natural gas in organic-rich tight shales is extracted by creating a network of fractures in the rock, known as hydraulic fracturing. This process involves injecting hydraulic fracturing fluid (HFF) into organic–rich shales, which is typically composed of makeup water (a base fluid used to transport the fracturing chemicals, which ranges in composition), proppant, and chemicals (e.g., Lee et al., 2011), under high enough pressure to create fractures.

* Corresponding author at: Department of Geology and Environmental Science, University of Pittsburgh, 4107 O'Hara St. 200SRCC, Pittsburgh, PA 15260, United States.
E-mail address: thaiphan@pitt.edu (T.T. Phan).
[1] Current address: Department of Earth and Environmental Sciences, University of Waterloo, 200 University Ave. W, Waterloo, Ontario, Canada N2L 3G1.

https://doi.org/10.1016/j.coal.2018.02.014
Received 22 August 2017; Received in revised form 16 February 2018; Accepted 16 February 2018
Available online 19 February 2018
0166-5162/

Recent studies reported reactions between HFF and shale that could affect reservoir porosity and permeability, and thus potentially affect long-term production of hydrocarbons from fractured unconventional formations (Dieterich et al., 2016; Harrison et al., 2017; Marcon et al., 2017; Paukert Vankeuren et al., 2017; Tasker et al., 2016; Wilke et al., 2015). HFF-shale reactions observed include: calcite dissolution and release of trace elements into solution; increases in dissolved sulfate from pyrite oxidation and ammonium persulfate reduction (in cases where ammonium persulfate is used as a gel breaker compound in the HFF) leading to formation of sulfate mineral scale (Paukert Vankeuren et al., 2017); and formation of secondary minerals at later stages of HFF-shale exposure due to changes in pH and redox conditions (Dieterich et al., 2016; Marcon et al., 2017; Tasker et al., 2016; Wilke et al., 2015), such as precipitation of Fe(III)-bearing secondary minerals derived from oxidation of Fe(II)-bearing phases in shale (Jew et al., 2017; Pearce et al., 2018). Experimental determination of HFF-shale reactions usually combines analysis of both reacted fluids and rock surfaces. In the field, however, recovery and analysis of the reacted rock surface is not feasible so HFF-shale reactions must be ascertained solely through the chemistry of flowback and produced waters (waters co-produced with oil and gas during early and long-term production, respectively). Identifying geochemical tracers in these waters that can distinguish between water − rock reactions, HFF mixing with formation water, and salt diffusion of in situ brines into HFF, will be critical for monitoring HFF − shale reactions in hydraulically fractured reservoirs.

The focus of this study is to investigate the applicability of Li isotopes (δ^7Li), radiogenic Sr isotopes (ε_{Sr}^{SW}), and U concentration as geochemical tracers of HFF-shale reactions. This was performed by analyzing effluents from laboratory − scale core flood experiments designed to study HFF − shale reactions (Paukert Vankeuren et al., 2017), in order to identify relationships between changes in chemical tracers in the effluent and observed mineral changes in the reacted shale. Results from this analysis are then compared to published data on produced water chemistry and sequential extractions from Marcellus Shale to determine whether HFF − shale reactions identified by the tracers could be distinguished from the chemical influence of brine diffusion or mixing into the hydraulic fractures in field − collected produced water samples. The results of this study will be used to evaluate whether water − rock interactions in hydraulically fractured shale at depth can be identified by monitoring δ^7Li, ε_{Sr}^{SW}, and U concentration in Marcellus Shale produced waters.

2. Background

Increases in concentration of total dissolved solids (TDS) in produced water generated from fractured unconventional reservoirs could indicate interaction with formation water or contact between injected HFF and the shale. Ions that comprise the bulk of solution chemistry, such as Na, Ca, and Cl, could be added through brine diffusion (Balashov et al., 2015), brine mixing (Haluszczak et al., 2013; Capo et al., 2014; Rowan et al., 2015; Phan et al., 2016), or water − rock reactions. Reaction − specific isotopes and trace elements may be useful for teasing out the relative importance of these processes. Certain metal isotopes (e.g., ^{7}Li/^{6}Li, ^{87}Sr/^{86}Sr) and trace elements (U) have been used to characterize the origin of formation water in the Marcellus Shale. Moreover, they may be subject to changes during HFF − shale reaction that can indicate carbonate and clay mineral dissolution, and secondary precipitation of clays and scale-forming minerals.

Li and radiogenic Sr isotopes are useful tracers of the sources of the dissolved solids in Marcellus Shale produced water and fluid mixing in the fractured shale reservoir (Capo et al., 2014; Macpherson et al., 2014; Stewart et al., 2015; Phan et al., 2016), but the effect of water-rock interactions on the isotopic compositions of these two elements during hydraulic fracturing of Marcellus Shale has not been fully evaluated. Structurally bound Li (e.g., Li in clays) accounts for 75–91 wt.% of total Li in Marcellus Shale whereas negligible Li (< 3%) is extracted from exchange sites and carbonate cement (Phan et al., 2016). Up to 20% of Li is released from the oxidation of sulfide minerals (e.g., pyrite) and organic matter (Phan et al., 2016). Thus, monitoring Li in laboratory HFF-shale experiments is expected to provide insight into the contribution of ion exchange and oxidation reactions towards produced water chemistry. Similarly, Stewart et al. (2015) showed that Sr associated with water soluble, exchangeable, and carbonate components can contribute to up to 77% of total Sr in whole rock of Marcellus Shale. These sources can release Sr into produced water from shale rock during hydraulic fracturing, particularly from the dissolution of carbonate minerals near the well. The ε_{Sr}^{SW} values in the water-soluble component is similar to the range of ε_{Sr}^{SW} values in Marcellus produced water, while the ε_{Sr}^{SW} values of the exchangeable and carbonate components are distinct from produced water and each other (Stewart et al., 2015). Therefore, monitoring changes in ε_{Sr}^{SW} is expected to provide insight into ion exchange and carbonate mineral reactions in laboratory experiments.

U concentration may also be a valuable tracer of HFF-shale reactions. The primary species of U is sensitive to both redox and pH, and may act as an indicator of geochemical conditions in the reservoir as well as water-rock reaction. U exists primarily as U(VI)–carbonate complexes under oxidizing conditions, with the specific uranyl–carbonate complexes varying in form depending on the pH and the proportion of other complex forming ions (Langmuir, 1978). For example, depending the concentration of Ca^{2+}, U exists as a complex of either $Ca_2UO_2(CO_3)_3$ or $CaUO_2(CO_3)^{2-}$ under alkaline pHs (Dong and Brooks, 2006). Under reducing conditions, U(IV) is the primary species, which is found in insoluble minerals such as uraninite (U_3O_8) (Suzuki et al., 2002). U can also be removed from the aqueous phase by adsorption onto minerals such as metal-oxyhydroxides (Hsi and Langmuir, 1985) and clays (Sylwester et al., 2000). In the Marcellus Shale, U is present at concentrations from 5 ppm to 90 ppm (Phan et al., 2015; Wendt et al., 2015), with carbonate minerals containing up to 20% of the total U (Phan et al., 2015). However, U in produced waters collected from hydraulically fractured Marcellus Shale (Phan et al., 2015) is very low ($< 4\ \mu g\ L^{-1}$), with the highest concentration observed in water samples collected on the first day of flowback (Phan et al., 2015). High U in these samples was explained by either the dissolution of carbonate minerals near the well during hydraulic fracturing, or U pre − existing in the makeup water (Phan et al., 2015). Laboratory − scale HFF-shale experiments, combined with reactive transport modeling of U–bearing mineral dissolution, may elucidate whether carbonate dissolution contributes towards the U pulse observed in early-stage flowback waters from the Marcellus Shale.

3. Methods

3.1. Description of core flood experiments

Core flood experiments were conducted at elevated temperature and pressure (66 °C, 20 MPa pore pressure), designed to simulate typical conditions within Marcellus Shale gas wells in southwestern Pennsylvania, USA. A schematic diagram of the experimental setup is shown in Fig. 1 and described in additional detail in Paukert Vankeuren et al. (2017). Cores for the experiments (15.2 cm in length, 3.8 cm in diameter) were cut from the interior of large shale blocks collected from an excavated area in New Bedford, PA, approximately 1.5 m below the surface and 0.6 m into the hillside (Paukert Vankeuren et al., 2017) to minimize weathering. Outcrop samples were used because of limited availability of fresh drill core. Though surficial weathering, e.g., pyrite dissolution and organic matter decomposition, has been observed in outcrop samples from nearby localities (e.g., Heidari et al., 2017; Jin et al., 2013; Petsch et al., 2000), scanning electron microscope images of our shale outcrop samples show persistent pyrite and organic matter (Paukert Vankeuren et al., 2017). Additionally, even if weathering caused some organic matter loss in the outcrop samples, this would not

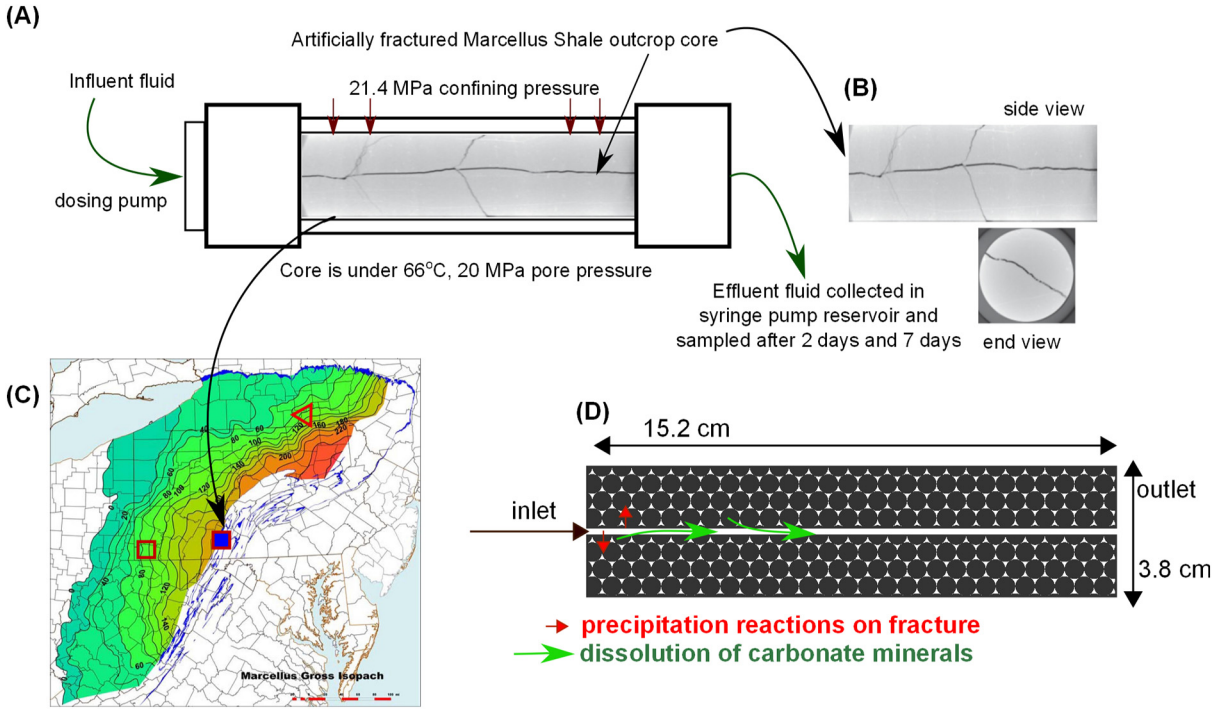

Fig. 1. Schematic diagram of the flow–through experimental apparatus (A) and an example of x-ray CT images of an unreacted and artificially fractured core (B). Marcellus isopach map (C) (Milici and Swezey, 2006) shows the locations of outcrop shale samples in Bedford, PA, USA (filled square), and core shale samples in Greene County, PA (open square) and Tioga County, NY, USA (open triangle). A conceptual model of the dual porosity medium of the reactive transport modeling (D).

likely affect the U content. Even though a positive correlation between U and total organic carbon (TOC) was observed in deep cores of Marcellus Shale (e.g., Phan et al., 2015; Wang and Carr, 2012), the correlation is attributed to the accumulation of both U and TOC under an anoxic environment (e.g., Phan et al., 2018). U is mainly present as uraninite in Marcellus Shale (Fortson, 2012) and thus U should not be affected by later loss of organic matter. Futhermore, prior investigation demonstrated that the difference in elemental composition and mineralogy between sub-surface core and outcrop samples of Marcellus Shale such as those used in this study is not statistically significant (Noack et al., 2015). Therefore, the major mineral reactions observed using outcrop samples should be representative of those that occur in shale at depth.

A total of five fluids with different chemical compositions (Table 1) were used to represent typical hydraulic fracturing processes with fresh water (spring water experiments SW and SWF) and diluted produced water (experiments PW, PWF, and PWFNA). For all experiments, local fresh water (sourced from Moshannon, Pennsylvania, USA) was used as the base fluid for preparing the HFF solutions in order to emulate water sources used for regional hydraulic fracturing operations. To represent conditions in which operators use diluted produced water as the HFF base fluid, salts were added to the local fresh water to match dissolved solids concentrations in HFF samples provided by an operator partner with wells in the Marcellus Shale (PW). Fracturing chemicals were added to these two base fluids, including hydrochloric acid (HCl) (SWF and PWF) in order to represent near–wellbore conditions where residual acid may be present from acid injection performed to clean the well perforations prior to hydraulic fracturing. One fluid was prepared with fracturing chemicals and without acid (PWFNA) to represent conditions farther from the wellbore. Two of the fluids (SWF and PW) were spiked with Li (LSVEC standard) to a concentration of approximately 1 mg L^{-1} Li to aid in interpretation of changes in $^{7}Li/^{6}Li$ ratio. A summary of the experiments is presented in Table 1, and detailed chemistry of the fluids is presented in the Supporting Information of Paukert Vankeuren et al. (2017).

Table 1
Summary of the flow–through experiments conducted at 66 °C, 20 MPa.

Experiment	Fluid type	Orientation of fracture to bedding planes
SW0	Fresh spring water (control)	No rock
SW 1	Fresh spring water	Parallel
SW 2	Fresh spring water	Perpendicular
SWF0	Fresh spring water based HFF with HCl	No rock
SWF1	(control)	Parallel
SWF2	Fresh spring water based HFF with HCl	Perpendicular
	Fresh spring water based HFF with HCl	
PW0	Synthetic produced water (control)	No rock
PW1	Synthetic produced water	Parallel
PW2	Synthetic produced water	Perpendicular
PWF0	Synthetic produced water based HFF	No rock
PWF1	with HCl (control)	Parallel
PWF2	Synthetic produced water based HFF	Perpendicular
	with HCl	
	Synthetic produced water based HFF	
	with HCl	
PWFNA0	Synthetic produced water based HFF	No rock
PWFNA 1	(control)	Parallel
PWFNA 2	Synthetic produced water based HFF	Perpendicular
	Synthetic produced water based HFF	

Cores were artificially fractured, and quartz sand proppant was placed along the primary fracture prior to loading the cores into the core flood apparatus. For each fluid type, experiments were conducted with cores fractured both parallel and perpendicular to bedding planes. For each experiment containing shale, two core plugs (15.2 cm in length, 3.8 cm in diameter) were placed lengthwise in rubber sleeves and mounted in a Hassler–type core flood apparatus. A detailed description of the core placement and the experimental apparatus is presented in Paukert Vankeuren et al. (2017). Each unique fracture fluid (listed above; Table 1) was reacted using a freshly-prepared shale sample. Fresh unreacted fluid was continuously drawn from an influent reservoir and pumped through the core at a rate of 2.4 mL hr^{-1} and the

effluent was collected in syringe pump reservoirs. Headspace above the initial fluid (also referred to as influent) was maintained with N_2 in order to replicate anoxic conditions in the subsurface. Cumulative effluents were collected after 2 days and 7 days from the start of the experiment and analyzed. Prior to performing experiments with the shale core, control experiments were performed using the same core flood apparatus but with stainless steel spacers in place of the shale core to evaluate changes to fluid chemistry in the absence of shale.

3.2. Sequential extractions of Marcellus shale

To assist our understanding of chemical reactions occurring in the flow − through experiments, we analyzed the sequentially extracted leachates of core materials of Marcellus Shale for radiogenic Sr isotopes and elemental concentrations. This information is also expected to aid in understanding water − rock interactions during hydraulic fracturing of Marcellus Shale. The leachate samples include water soluble, exchangeable, and carbonate fractions of Marcellus Shale, which were archived from a previous study (Phan et al., 2015). The drill core materials were collected from varying depths covering both Oatka Creek and Union Springs members of Marcellus Shale from two sites: Greene County, PA, USA and Tioga County, NY, USA (Fig. 1). In addition, elemental and $^{87}Sr/^{86}Sr$ data of the leachates of Marcellus shale rocks reported in Stewart et al. (2015) are used for comparison.

It is important to note that the sequential extraction was performed on limited number of shale samples (8 in total) from drill cores whereas the shale material used in the core flood experiments were collected from outcrop. As discussed in Section 3.1, major mineralogy of outcrop samples is not expected to differ significantly from drilled cores due to weathering. However, previous studies showed that mineralogical composition, including the carbonate content in Marcellus Shale, can differ spatially and stratigraphically (Wang and Carr, 2012; Jin et al., 2013; Phan et al., 2015; Stewart et al., 2015). For example, carbonate content (as $CaCO_3$) in Oatka Creek and Union Springs members of Marcellus Shale was mostly < 5% (Phan et al., 2015) whereas calcareous shale containing carbonate veins within Marcellus Shale can contain up to 65% carbonate (Jin et al., 2013). Because much of the Sr in Marcellus Shale is found in calcium carbonate minerals (Stewart et al., 2015), Sr results are normalized by the Sr/Ca ratio to account for differences in carbonate content. This normalization allows for comparison of Sr results from outcrop samples in flow-through experiments and drilled core in sequential extractions.

3.3. Analytical techniques

3.3.1. Cation and anion concentrations

Experimental water samples were filtered through 0.45 μm membrane syringe-tip filters (SFCA membrane, Cole-Parmer) and acidified with ultra-pure HNO_3 (Optima grade, Fisher) prior to elemental analysis by inductively coupled plasma mass spectroscopy (ICP–MS; Perkin-Elmer NexION 300X) and optical emission spectroscopy (ICP-OES). Samples for major anion analysis by ion chromatograph (IC) were filtered through 0.2 μm membrane syringe-tip filters (Acrodisc PF Supor Membrane, Pall). Major elemental data of effluent samples from the core flood experiments are reported in Paukert Vankeuren et al. (2017); this study reports the concentrations of Li, Sr, and U. The concentrations of some elements relevant to the discussion in this work are given in Table 2 and shown in a Piper plot (Fig. 2). In this study, the metal concentrations in Marcellus shale sequential extraction leachates were measured by ICP–MS at the University of Pittsburgh. The estimated accuracy of elemental data was better than 10% based on replicate measurements of reference materials (groundwater standards NIST1640a and ESL-2).

3.3.2. Strontium isotopes

Sample matrix separation for Sr isotopes using Sr–Resin (Eichrom, USA) followed the high-throughput method described in Wall et al. (2013). Sr isotope measurements were performed on the Neptune plus multi-collector inductively coupled plasma mass spectrometer (MC–ICP–MS). The measured $^{87}Sr/^{86}Sr$ ratio was normalized to SRM-987 standard = 0.710240 and reported both as $^{87}Sr/^{86}Sr$ ratio and ε_{Sr}^{SW} relative to sea water,

$$\varepsilon_{Sr}^{sw} = \left(\frac{^{87}Sr/^{86}Sr_{sample}}{^{87}Sr/^{86}Sr_{seawater}} - 1 \right) \times 10^4 \quad (1)$$

where $^{87}Sr/^{86}Sr_{seawater}$ is the measured ratio of modern seawater. In this study, we use the value measured at the University of Pittsburgh as the seawater standard: $^{87}Sr/^{86}Sr_{seawater} = 0.709166$ (Chapman et al., 2012).

For data quality control, two reference standards, UD6 − 120518 − S (produced water) and EN-1 ($CaCO_3$, shell of giant clam Tridacna gigas, USGS standard), were processed together with water samples in each chemistry session during the course of the study. The in-house standard UD6–120518-S (produced water) yielded $^{87}Sr/^{86}Sr = 0.719958 \pm 0.000020$ (2SD; n = 9), which agrees well with our previously reported values (0.719956 ± 0.000041; n = 8) (Kolesar Kohl et al., 2014; Phan et al., 2016). Likewise, repeated measurement of EN − 1 in this study yielded $^{87}Sr/^{86}Sr = 0.709159 \pm 0.000032$ (n = 9) which is consistent with the value 0.709169 reported in Neymark et al. (2014), when their measured $^{87}Sr/^{86}Sr$ is normalized to 0.710240. Reproducibility of column duplicate was 0.2 ε unit (or 0.02‰) on average (n = 32).

3.3.3. Lithium isotopes

Lithium isotopes (^6Li and ^7Li) were separated from the sample matrix prior to analysis on a MC − ICP − MS following the method reported in Phan et al. (2016). We also applied a novel rinsing procedure using 5% NaCl for 1 min after 4 to 6 h of analytical session; this was shown to effectively wash out Li (Lin et al., 2016), thus, improving the precision of the measurements. In order to prevent potential issues with the extraction lenses, the skimmer valve was closed during the introduction of 5% NaCl solution. The measured $^7Li/^6Li$ ratio is reported as:

$$\delta^7Li = \left(\frac{^7Li/^6Li_{sample}}{^7Li/^6Li_{LSVEC}} - 1 \right) \times 10^3 \quad (‰) \quad (2)$$

where $^7Li/^6Li_{LSVEC}$ is the average $^7Li/^6Li$ ratio of SRM − 8545 (LSVEC) standard (Li_2CO_3) measured before and after the sample. An in-house standard WA–A25 (Marcellus Shale produced water; University of Pittsburgh) was measured to check for reproducibility during the course of the study. For each sample, two separate aliquots were processed through the Poly-Prep columns (0.8 × 4 cm; Bio-rad) filled with 2 mL cation-exchange resin (AG50W-X8) prior to isotopic analysis. The δ^7Li and 2SD reported in Table 2 are the average value and two standard deviations of the column duplicate, respectively. In this study, measured δ^7Li of WA-A25 was 9.2 ± 0.1 (n = 2) which is consistent with our previous work (e.g., 9.5 ± 0.4, n = 5 (Phan et al., 2016); 9.4 ± 0.1, n = 2 (Macpherson et al., 2014)). Measurements of two separate aliquots gave precision better than 0.5‰ (2SD). It is necessary to ensure complete recovery of Li to prevent any potential isotope fractionation from the matrix separation procedure. For each sample, an aliquot of the purified lithium fraction, and aliquots from the ion-exchange-column collected before and after the purified lithium fraction were measured for Li and Na by ICP-MS to check for lithium column recovery and Na/Li mass ratio in the purified Li fraction. The recovery of all analyzed samples was > 99%. The Na/Li of all reported samples was < 5, which negligibly affects the measured δ^7Li (Bryant

Table 2
Elemental concentrations of water samples from the flow–through experiments and isotopic compositions (δ^7Li, ε_{Sr}^{SW}).

Sample ID[a]	pH[b]	Li	Sr	Ca[b]	SiO_2[b]	Al[b]	U	Li*10^3/Ca	Sr/Ca	Cl/Br	Na/Br	TZ^+[c]	δ^7Li ± 2SD[d]	$^{87}Sr/^{86}Sr$ ± 2SD[e]	ε_{Sr}^{SW} ± 2SD[f]
		mg L^{-1}					µg L^{-1}						‰		
SW-influent	5.1	0.005	0.014	1.24	3.90	< 0.01	< 0.2	3.83	0.011	3.8	4.8	0.31	–	0.714999	82.3
SW0-2	6.1	0.003	0.019	6.54	4.11	0.03	< 0.2	0.466	0.003			0.85	–	0.713033	54.5
SW1-2	6.6	< 0.002	0.096	55.7	8.56	0.07	7.2	–	0.002	22	21	6.14	–	0.709185 ± 0.000007	0.3 ± 0.1
SW1-7	6.9	< 0.002	0.070	42.9	8.12	0.07	5.4	–	0.002	10	14	4.84	–	0.709211 ± 0.000003	0.6 ± 0.0
SW2-2	6.5	< 0.002	0.101	56.7	9.31	0.04	< 0.2	–	0.002	13	13	6.23	–	0.709156 ± 0.000018	−0.1 ± 0.2
SW2-7	7.2	0.011	0.088	23.7	6.16	0.12	2.3	0.474	0.004	5.0	16	2.91	–	0.709601	6.1
SWF-influent	1.7	1.31	0.047	2.05	3.97	0.31	< 0.2	640	0.023			4.46	−0.6 ± 0.7	0.707876	−18.2
SWF0-2	1.7	1.31	0.808	31.8	5.49	1.02	< 0.2	41.1	0.025	2486	79	7.95	−0.1 ± 1.1	0.708024 ± 0.000014	−16.1 ± 0.2
SWF1-2	3.1	1.30	1.34	583	11.1	1.03	67	2.23	0.002	2320	59	64.9	0.1 ± 0.4	0.708202 ± 0.000036	−13.6 ± 0.5
SWF1-7	6.5	1.31	1.33	542	9.01	1.11	44	2.41	0.002	2889	68	61.1	0.0 ± 0.1	0.708148 ± 0.000023	−14.4 ± 0.0
SWF2-2	2.9	1.30	1.25	586	8.56	1.73	48	2.22	0.002	2543	61	65.2	−0.6 –	0.708157 ± 0.000003	−14.2 ± 0.3
SWF2-7	7.2	1.32	1.40	611	6.60	0.79	35	2.16	0.002	3292	73	67.9	−0.2 ± 0.4	0.708115 ± 0.000059	−14.8 ± 0.8
PW-influent	7.2	1.37	443	1940	3.52	0.81	5.3	0.705	0.229	105	44	500	1.6 ± 0.2	0.707813 ± 0.000005	−19.1 ± 0.1
PW0-2	7.7	1.34	453	1850	4.23	0.83	1.3	0.721	0.244	106	44	490	1.9 ± 0.2	0.707814 ± 0.000009	−19.1 ± 0.1
PW1-2	7.3	1.40	441	1960	9.00	0.80	12	0.716	0.225	109	45	501	1.6 ± 0.1	0.707809 ± 0.000008	−19.1 ± 0.1
PW1-7	7.5	1.33	448	1960	6.95	0.80	5.4	0.682	0.229	108	45	501	1.8 ± 0.1	0.707807 ± 0.000003	−19.2 ± 0.1
PW2-2	7.5	1.31	444	2000	6.57	0.86	8.0	0.653	0.222	112	47	509	2.2 ± 0.4	0.707810 ± 0.000006	−19.1 ± 0.0
PW2-7	7.9	1.33	452	1900	4.70	0.84	3.6	0.701	0.238	107	45	496	1.9 ± 0.3	0.707807 ± 0.000001	−19.2 ± 0.0
PWF-influent	2.0	0.252	450	1920	3.40	0.98	1.4	0.131	0.234	114	45	508	–	0.707809 ± 0.000010	−19.1 ± 0.1
PWF0-2	2.1	0.185	420	1890	4.42	1.06	1.9	0.098	0.222	114	45	494	–	0.707810 ± 0.000005	−19.1 ± 0.1
PWF1-2	4.6	0.449	429	2430	9.60	1.37	57	0.185	0.177	115	45	557	–	0.707817 ± 0.000024	−19.0 ± 0.3
PWF1-7	6.2	0.385	434	2370	8.71	1.68	37	0.163	0.183	115	45	550	–	0.707811 ± 0.000021	−19.1 ± 0.3
PWF2-2	3.8	0.463	428	2370	7.25	1.38	42	0.196	0.181	113	44	544	–	0.707803 ± 0.000003	−19.2 ± 0.0
PWF2-7	6.0	0.324	442	2470	6.65	1.53	32	0.131	0.179	115	45	564	–	0.707821 ± 0.000002	−19.0 ± 0.0
PWFNA-influent	8.2	0.337	453	2030	3.57	0.80	1.4	0.166	0.223	107	45	517	–	0.707806 ± 0.000005	−19.2 ± 0.1
PWFNA0-2	7.7	0.271	437	1830	4.52	0.81	1.8	0.149	0.239	107	45	487	–	0.707808 ± 0.000019	−19.2 ± 0.3
PWFNA1-2	7.7	0.275	434	2070	9.46	0.88	19	0.133	0.210	107	45	517	–	0.707809 ± 0.000004	−19.1 ± 0.1
PWFNA1-7	7.5	0.275	443	2060	6.11	0.82	4.1	0.134	0.216	106	45	522	–	0.707810 ± 0.000005	−19.1 ± 0.1
PWFNA2-2	7.7	0.249	431	2090	7.36	0.95	13	0.119	0.206	108	45	517	–	0.707807 ± 0.000010	−19.2 ± 0.1
PWFNA2-7	7.4	0.167	447	1930	4.74	0.84	1.8	0.087	0.231	107	45	514	–	0.707813 ± 0.000011	−19.1 ± 0.2

[a] The first part of the sample ID denotes the experiment (see Table 1 for descriptions), the last number denotes the time of sample collection in number of days since the start of the experiment.
[b] As reported in Paukert Vankeuren et al. (2017).
[c] $TZ^+ = Na^+ + 2\,Mg^{2+} + K^+ + 2Ca^{2+}$ as milliequivalent per liter, mEq L^{-1}.
[d] 2SD = two standard deviations of full procedural replicates (two or three separate aliquots of the same sample were independently processed through cation exchange resin for matrix separation).
[e] SRM987 Sr standard = 0.710240; 2SD = two standard deviations of full procedural replicates.
[f] $\varepsilon_{Sr}^{SW} = (^{87}Sr/^{86}Sr_{sample}/^{87}Sr/^{86}Sr_{seawater} - 1)10^4$ where $^{87}Sr/^{86}Sr_{seawater} = 0.709166$.

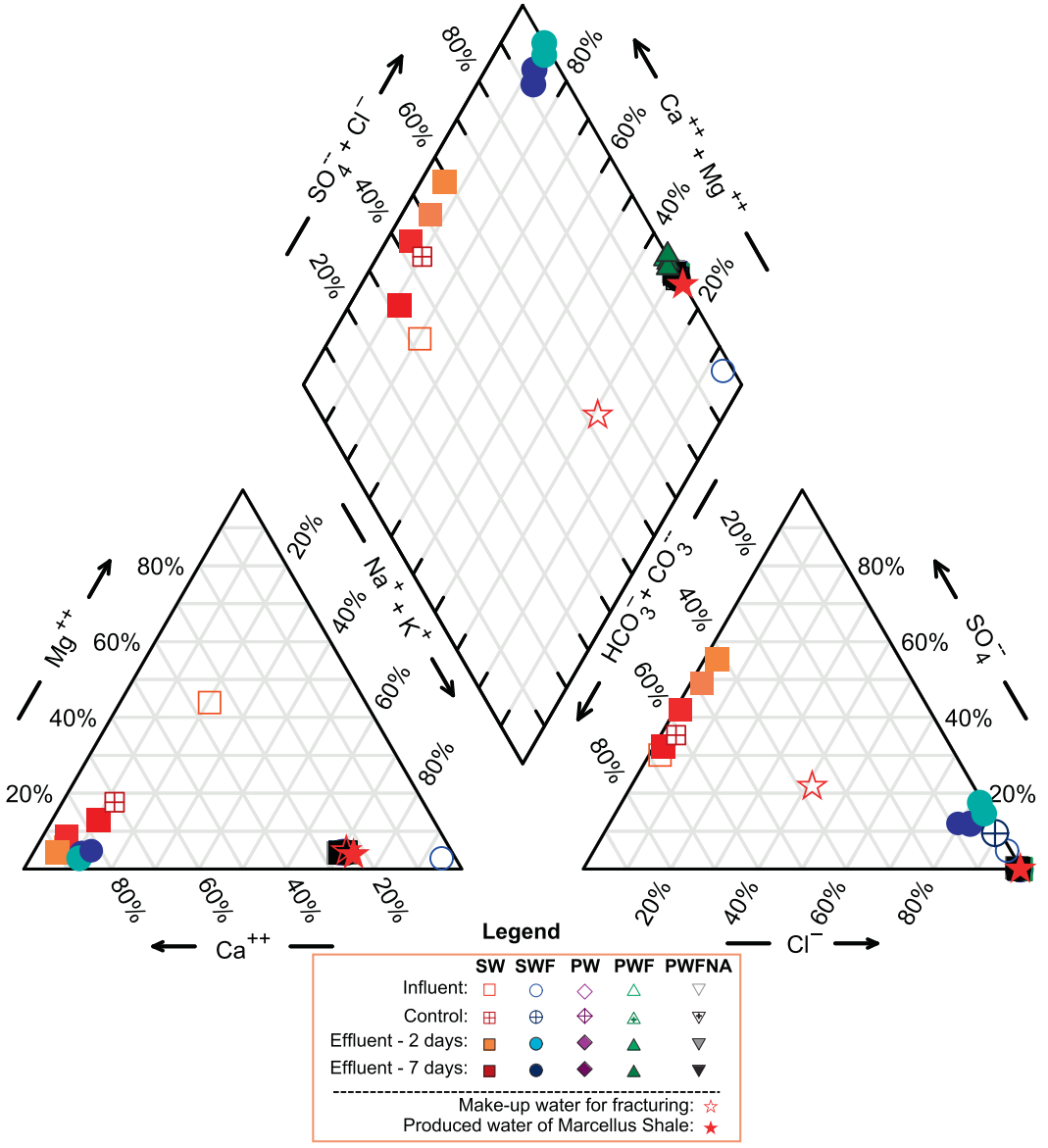

Fig. 2. Piper diagram (Piper, 1944) of water samples from the flow – through experiments. Marcellus produced water (median values) and make up water used for hydraulic fracturing (Hayes, 2009; Rowan et al., 2015) are shown for comparison. Concentrations of major ions in the core flood experimental samples are reported in Paukert Vankeuren et al., (2017).

et al., 2003). Overall, the estimated uncertainty of δ^7Li was better than 0.5‰. In this study, lithium isotope analysis was performed on select samples to determine effects of major mineral reactions on the δ^7Li in the reacted fluid. Samples from SWF experiments were analyzed to evaluate the effect of acidic dissolution of shale carbonate minerals, and samples from PW experiments were analyzed to investigate desorption of Li from exchange sites of shale minerals at circumneutral pH (See 5.2 for Discussion).

3.4. Reactive transport modeling

Reactive transport modeling was carried out in this study to investigate the maximum extent of U that could be released during the flow-through experiments due to dissolution reactions involving U–bearing minerals and calcite in the presence of HFF (Experiments SWF and PWF, Table 2). Equivalent one linear dimensional (1D) models of the reactive transport of experimental fluids along the artificially fractured porous rock were performed using the reactive transport module X1t, Geochemist's Workbench (GWB) version 10 (Bethke, 2008). The updated thermodynamic database from thermo.com.v8.r6 + (Phan et al., 2015) was used in this study. A dual porosity (fracture geometry) model was selected to simulate two zones of fluid flow mimicking those in the flow-through experiments: one along the fracture, and one of stagnant fluid trapped in the porous rock material. We chose the fraction of the stagnant zone (X_{stag} = 95%) and half-width (δ = 0.76 cm; the width of slabs separated by fractures) to achieve the surface area per unit volume of the domain A_s = 1.25 $cm^2\ cm^{-3}$, which was within the estimated range of A_s (1.0–1.5 $cm^2\ cm^{-3}$) for artificially fractured cores used in the experiments. The porosity of the stagnant zone Φ = 0.08 (8%) was selected based on the total measured porosity of Marcellus Shale reported in Cipolla et al. (2010).

Minerals considered for dissolution reactions in the models include the primary minerals calcite, pyrite, chlorite, illite, smectite as nontronite-Na, quartz, and K-feldspar, and two uranium minerals, uraninite (U_3O_8) and uranophane ($Ca(UO_2)_2(HSiO_4)_2.5H_2O$). The volume fractions of the considered minerals were selected after Hosterman and Whitlow (1983), Wang and Carr (2012), and Phan et al. (2015). Paukert Vankeuren et al. (2017) found that mineralogical composition of the

Table 3
Input values for the reactive transport models for (a) the two flow-through experiments and (b) the kinetic parameters of the considered minerals that are allowed to react.

(a) The chemical compositions of inlet fluids (mg L^{-1})

Inlet fluid	pH	$O_{2(aq)}$	$CO_{2(aq)}$	Na^+	K^+	Mg^{2+}	Ca^{2+}	Ba^{2+}	Fe^{2+}	Al^{3+}	UO_2^{2+}	Cl^-	SO_4^{2-}	$SiO_{2(aq)}$
SWF-Influent	1.7	0.08192	0.00528	20.3	123.23	1.31	2.1	2.04	0.5	0.31	0.00023	958.39	75.41	3.97
PWF-Influent	2.0	0.08192	0.00528	6319	232	212	1924	225	1.0	1.0	0.00157	16,045	48.14	3.40

(b) Kinetic parameters

Primary minerals	X[a]	A, $m^2 g^{-1}$	k_{25}, mol $m^{-2} s^{-1}$	Ea, kJ mol^{-1}	k+, mol $m^{-2} s^{-1}$
Calcite	0.15	0.001			5.61×10^{-4}
Pyrite	0.05	0.00129	3.02×10^{-8}	56.9	
Chlorite	0.05	0.00098	7.762×10^{-12}	88	
Illite	0.33	0.01516	1.047×10^{-11}	23.6	
Smectite (Nontronite-Na)	0.05	0.01516	4.3652×10^{-12}	62.76	
Quartz	0.19[d]	0.02[d]	4.5×10^{-14}[d]	72.0[d]	
K-feldspar	0.01	0.11[e]	2.3×10^{-13}[f]	51.7[g]	
Uranium containing minerals					
Uraninite	0.00001[b]	0.005			4.83×10^{-10}[h]
Uranophane	0.00001[b]	0.005[c]			1.1×10^{-12}[i]

X = Mineral volume fraction of solid; A = mineral surface areas ($cm^2 g^{-1}$); k25 = kinetic dissolution rate constant at 25 °C (mol $m^{-2} s^{-1}$). All kinetic data were taken from Xu et al. (2006) except where noted.

[a] After Hosterman and Whitlow (1983) and Wang and Carr (2012).
[b] Estimated based on the average U concentration in Marcellus Shale (Phan et al., 2015).
[c] No available data; thus, the value of uraninite was used.
[d] Rimstidt and Barnes (1980).
[e] Gautier et al. (1994).
[f] Brantley (2008).
[g] Palandri and Kharaka (2004).
[h] Ulrich et al. (2009).
[i] Casas et al. (1994).

Marcellus Shale used for the core flood experiment varies slightly along the exposed surface fracture. Thus, the volume fractions of minerals considered in the models represent the average mineralogical composition of the fracture surface exposed to HFF. Both uraninite and uranophane were included in the reactive transport model because the presence of uraninite in the Marcellus Shale has been documented (Fortson, 2012), and uranophane may be present as a secondary mineral derived from weathering of outcrop shale (Pearcy et al., 1994). We previously observed that negligible U was extracted from the exchange sites of shale minerals (Phan et al., 2015); thus, adsorption is not considered in the models.

The model inputs include the chemical compositions of inlet fluids of experiments SWF and PWF, fluid flow rate, porosity, minerals allowed to react, surface area, and kinetic parameters (Table 3). The kinetic dissolution rate constant used for calcite was calculated following the pCO_2-dependent equation reported in Pokrovsky et al. (2009) for a pH of 4 and water temperature of 60 °C, similar to our experimental conditions. The headspaces of the inlet solutions (SWF-Influent and PWF-Influent) were filled with N_2 during the course of the experiments. Assuming that the mixture contains trace amount of air (1%), the calculated pCO_2 of the inlet fluid using Henry's law was 5.4 (P = 0.00000398 atm). For quartz and K-feldspar, the kinetic rate constants at 66 °C were calculated using the Arrhenius equation (Lasaga, 1984):

$$k_T = k_{25} \cdot \exp\left[-\frac{Ea}{R}\left(\frac{1}{T} - \frac{1}{298.15}\right)\right] \quad (3)$$

where k_{25} is the rate constant (mol $s^{-1} m^{-2}$) of a given mineral at 25 °C, R is the gas constant (8.314 J $mol^{-1} K^{-1}$), E_a is the activation energy (J mol^{-1}) of the given mineral and T is absolute temperature (K). The k_{25} and E_a values for quartz and K-feldspar were similar to the ones compiled in Hellevang et al. (2013). The kinetic dissolution rate of uraninite for carbonate rich and moderately oxidizing conditions was selected (Ulrich et al., 2009), representing the dissolved oxygen concentration (Henry's law for P_{O2} = 0.002 atm, which is equivalent to a mixture of 1% air and 99% N_2) in the inlet fluids, and the carbonate-rich conditions resulting from calcite dissolution in the experiments. The kinetic rate for uranophane was from Casas et al. (1994). Kinetic rates for pyrite, chlorite, smectite-Na, and illite were taken from acid-catalyzed mechanism rates reported in Xu et al. (2006). A conceptual 1D reactive transport model is shown in Fig. 1D.

4. Results

4.1. Elemental concentrations and ε_{Sr}^{SW} of sequential extraction leachates

The elemental concentrations and ε_{Sr}^{SW} data of the leachates are reported in Table 4 and also shown in ternary plots (Fig. 3). The water leachate contains the highest concentration of Na compared to the exchangeable and carbonate fractions, and is dominated by Na in comparison to K and Ca. The relative proportion of these cations in the water-soluble component is the most similar to Marcellus produced water (blue shaded area, Fig. 3A) compared to exchangeable (pink shaded area, Fig. 3A) and carbonate components (green shaded area; Fig. 3A). K and Ca dominate the composition of cations in the exchangeable fraction (Fig. 3A). For the carbonate fraction, Sr/Ca in shales from PA, USA ranged from 0.001 to 0.002 which was slightly lower than Sr/Ca in shales from NY, USA (0.002 – 0.005). For comparison, the Sr/Ca in Marcellus produced water (~0.2; Chapman et al., 2012; Capo et al., 2014) is up to two orders of magnitude higher than Sr/Ca in carbonate leachates analyzed in this study.

Measurements of radiogenic Sr isotopes in the exchangeable and

Table 4
Concentrations of major and minor elements in sequentially extracted components and $^{87}Sr/^{86}Sr$ in the exchangeable and carbonate components of Marcellus shale rocks.

Sample ID	Depth	Water soluble fraction µg extracted/g of sample						Exchangeable fraction µg extracted/g of sample								Carbonate fraction µg extracted/g of sample										
	(m)	Na	K[a]	Mg	Ca	Sr	Ba[b]	Na	K	Mg	Ca	Sr	Ba[b]	$^{87}Sr/^{86}Sr$	ε_{Sr}^{SW}	Na	K	Mg	Ca[b]	Sr	Ba[b]	$^{87}Sr/^{86}Sr$	±	2SD[c]	ε_{Sr}^{SW}	± 2SD[c]
Greene County, PA, USA																										
G3	2380	782	62.5	146	858	11	1.4	148	87.9	258	4286	23.4	71.8	0.711048	27	46	32	738	25,100	42	15	ND[d]			ND[d]	
G4	2386	954	238	211	945	18	1.5	125	230	277	1031	21.4	102	0.712055	41	7.1	12	252	2850	1.8	3.8	ND[d]			ND[d]	
G5	2389	920	209	218	637	13	1.2	110	164	296	613.3	22.0	275	0.711733	36	3.9	11	92.4	1110	2.3	9.3	ND[d]			ND[d]	
G6	2398	800	59.0	184	442	10	2.2	137	132	383	1494	15.9	55.1	0.711546	34	29	39	2890	10,700	23	31	0.708734	±	0.000007	−6.1	± 0.1
Tioga County, NY, USA																										
T2	1337	676	28.0	72.7	165	12	2.6	77.8	156	202	810	50.7	371	0.710600	20	11	20	1070	4310	9.3	36	0.710046	±	0.000008	12.4	± 0.1
T3	1358	639	45.1	42.7	310	13	3.9	140	133	231	728	31.7	426	0.710207	15	14	12	694	3520	16	37	0.709885	±	0.000008	10.1	± 0.1
T4	1370	665	30.4	74.3	379	30	4.1	79.2	86.8	223	2919	59.2	213	0.709769	8.5	60	20	1580	32,700	77	35	0.708386	±	0.000001	−11.0	± 0.0
T5	1389	694	26.4	55.0	336	34	4.6	66.7	54.3	136	2709	41.0	125	0.709784	8.7	64	11	2610	70,200	120	30	0.708307	±	0.000012	−12.1	± 0.2
Min		639	26	43	165	10	1	67	54	136	613	16	55	0.709769	8.5	4	11	92	1110	2	4	0.708307			−12.1	
Max		954	238	218	945	34	5	148	230	383	4286	59	426	0.712055	41	64	39	2890	70,200	120	37	0.710046			12.4	

$\varepsilon_{Sr}^{SW} = (^{87}Sr/^{86}Sr_{sample}/^{87}Sr/^{86}Sr_{seawater} - 1)10^4$ where $^{87}Sr/^{86}Sr_{seawater} = 0.709166$

[a] Previously reported in Phan et al. (2018).

[b] Previously reported in Phan et al. (2015).

[c] Two standard deviations of full procedural replicates (two or three separate aliquots of the same sample were independently processed for matrix separation)

[d] ND = no data due to the limited availability of samples

carbonate fractions of Marcellus Shale samples showed that ε_{Sr}^{SW} of these two components are distinct from each other (Table 4). The ε_{Sr}^{SW} values of Sr associated with the exchange sites exhibited a large range ($\varepsilon_{Sr}^{SW} = +9 - +41$; $^{87}Sr/^{86}Sr = 0.70977–0.71206$) that was generally greater than ε_{Sr}^{SW} values of Sr associated with carbonate minerals ($\varepsilon_{Sr}^{SW} = -12 - +12$; $^{87}Sr/^{86}Sr = 0.70831–0.71005$). While the ε_{Sr}^{SW} values of Sr in carbonate minerals of shale samples from two study locations overlapped, the ε_{Sr}^{SW} values of the exchangeable fraction of shale samples from PA, USA ($\varepsilon_{Sr}^{SW} = +27 - +41$; $^{87}Sr/^{86}Sr = 0.71105–0.71206$) were more radiogenic than samples from NY, USA ($\varepsilon_{Sr}^{SW} = +9 - +20$; $^{87}Sr/^{86}Sr = 0.70977–0.71060$).

4.2. Elemental concentrations and ε_{Sr}^{SW} in laboratory-scale core flood experimental effluents

Sr concentrations in core flood experimental effluents increased in concentration relative to the influent for the fresh water−based experiments (SW, SWF). Sr concentrations in the experimental effluents for all experiments performed with diluted produced water were similar to the control experiments (Fig. 4).

A shift in ε_{Sr}^{SW} values from the influent to the effluent was only observed in experiments with fresh water−based fluids (SW and SWF; Table 2; Fig. 4A, B) whereas the ε_{Sr}^{SW} value in experiments with diluted produced water−based fluids remained constant (Table 2; Fig. 4C, D, E). For the control experiment (SW0-2 Control), a large decrease by ~27 ε_{Sr}^{SW} units between influent (SW-Influent) and effluent (SW0-2 Control) was observed (Table 2; Fig. 4A). This change in ε_{Sr}^{SW} in the control is minor in comparison to the that in ε_{Sr}^{SW} in experiments with shale (SW), where a large decrease in ε_{Sr}^{SW} (~80 units) between the influent and effluent was measured (Table 2; Fig. 4A). In fresh water-based fluids containing both fracturing chemicals and acid (SWF), the ε_{Sr}^{SW} increased in the effluent relative to influent values (~4 epsilon units; Fig. 4B).

4.3. Elemental concentrations and δ^7Li in laboratory-scale core flood experimental effluents

Li concentrations in core flood experimental effluents remained similar to Li concentration in the influent for the fresh water−based experiments (with and without fracturing chemicals; SW and SWF), and in the diluted produced water-based experiment without fracturing chemicals (PW, Fig. 7). For the experiments performed with diluted produced water-based fluids with fracturing chemicals, in the case where acid was present, Li concentrations increased in both day 2 and day 7 effluents compared to the influent (PWF, Fig. 7). On the other hand, in the case where acid was not included (PWFNA), the difference in the changes in Li concentrations between control experiments and experiments with core material was not notable (Fig. 7).

Differences between the influent and effluent δ^7Li values are not statistically significant for core flood experiments performed with fresh water−based HFF (containing acid; SWF) (Table 2; Fig. 5A). All values are within the analytical uncertainty (2SD = 0.5‰). Similarly, no difference in δ^7Li was observed between the influent ($\delta^7Li = 1.6 \pm 0.2$‰) and effluents ($\delta^7Li = 1.9 \pm 0.5$‰, average of both day 2 and day 7 effluents) for core flood experiments performed with fluids representing diluted produced water (no acid; PW) (Table 2; Fig. 5B).

4.4. Changes in U concentration in laboratory-scale core flood experimental effluents

U in the effluents of core flood experiment SWF and PWF ranged from 32 to 67 µg L^{-1} whereas control experiments did not display any changes in U relative to the influent (< 1 µg L^{-1}). For both SWF and PWF experiments, U reached a maximum concentration of 67 µg L^{-1} in the day 2 effluents whereas the released U was lower in day 7 effluents

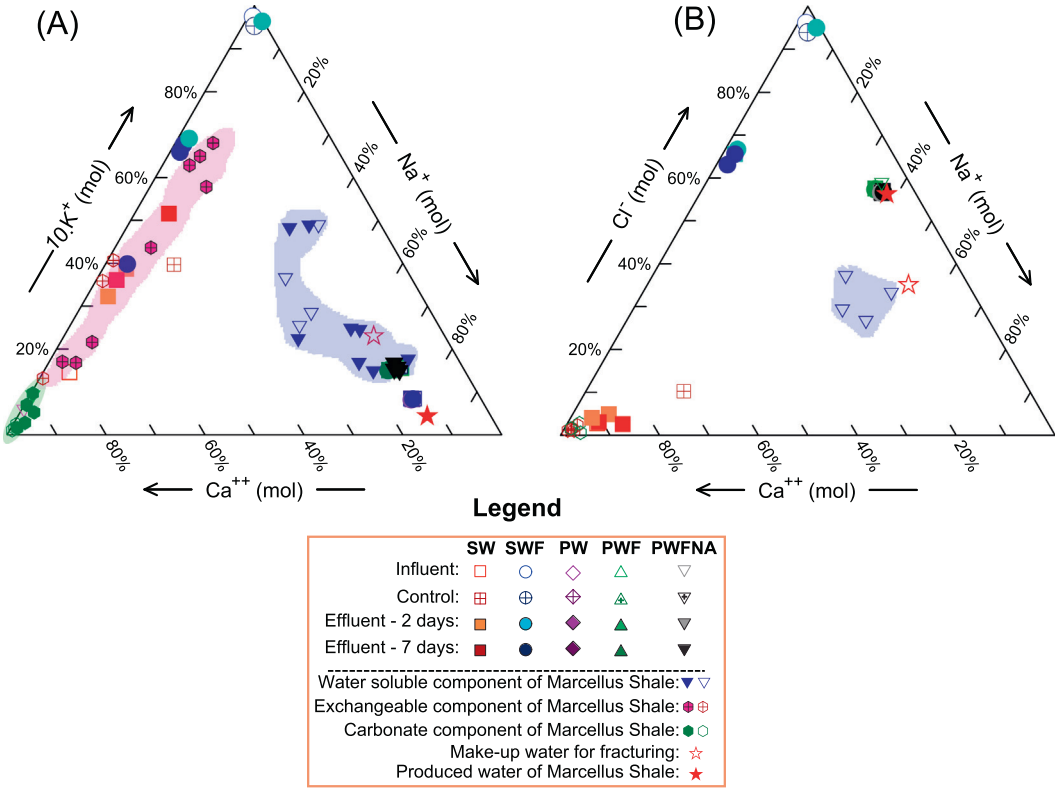

Fig. 3. Ternary diagrams comparing molar concentrations of Cl^-, Ca^{2+}, Na^+, and K^+ in the experimental fluids to water soluble (triangle down), exchangeable (crossed hexagon), and carbonate (hexagon) components of Marcellus Shale in this study (filled symbols) and from a previous work (open symbols; Stewart et al., 2015), and Marcellus produced water (Hayes, 2009; Rowan et al., 2015). Shaded regions highlight the boundary of the extracted components of Marcellus Shale.

(Table 2). Experiments that did not include HCl in the fluid showed much less dramatic increases in U, with maximum concentrations of 7–19 μg L^{-1}.

4.5. Results from modeling U release due to mineral reactions

Reactive transport model results showed that K-feldspar and quartz (potential U-bearing minerals), illite, chlorite, smectite, and pyrite did not react with the influent water under acidic conditions (horizontal lines, Fig. 6A, B), whereas extensive calcite dissolution occurred in both experiments within 6 cm from the inlet of the core (shaded area, Fig. 6A, B). Modeling results also show that dissolution of both uranophane and uraninite is unlikely to occur (Fig. 6A, B).

In SWF and PWF experiments, the influent solutions (SWF-Influent and PWF-Influent) were acidic (pH 1.7 and pH 2.0, respectively) and calculated Eh for both solutions was approximately 0.76 V (dropped to about −0.05 V as fluid flows towards the core). Prior studies (Casas et al., 1994; Torrero et al., 1997) showed that the dissolution of uraninite and uranophane is favored under acidic and oxidizing conditions. However, under the modeling conditions applied in this study, the dissolution of uraninite and uranophane were kinetically limited relative to calcite, and as such uraninite and uranophane were not considerable contributors of U to the solution. The model results showed that < 0.004% and 0.01% of both uraninite and uranophane were dissolved in experiments SWF and PWF, respectively. As shown in Fig. 6C and D, no notable difference is observed between the predicted concentrations of U in the reacted fluids and U in the influent (horizonal dashed arrow). Overall, geochemical modeling results indicate that calcite was the only mineral to experience substantial dissolution; the other minerals displayed no observable change in concentration (K-feldspar, quartz, illite, chlorite, smectite, pyrite, uraninite, and uranophane; horizontal lines in Fig. 6A, B).

5. Discussion

5.1. Application of Li as an indicator of HFF-shale reactions in core flood experiments

The δ^7Li values showed no change, or only change within analytical uncertainty, in experiments performed with both fresh water and diluted produced water as the make−up fluids in core flood experiments with Marcellus Shale. Two experiments were evaluated to consider potential changes in δ^7Li due to water-rock interaction: fresh water-based fluid containing HFF chemicals including acid (SWF), and synthetic diluted produced water without HFF chemicals (PW). SWF experiments were expected to show changes in δ^7Li due to carbonate mineral dissolution in acidic HFF. PW experiments were expected to show changes in δ^7Li due to ion exchange reactions between diluted produced water and shale, independent of carbonate mineral reactions.

For the SWF experiment, the lack of δ^7Li change in experimental effluent suggests that carbonate mineral reactions occurring during HFF–shale interactions may not produce a detectable effect on Li isotope composition in the effluents. Marcellus Shale carbonate cements are low in Li (< 1 ppm; Phan et al., 2016), and constant supply of Li (~1 mg L^{-1}) in the influent solution likely obscured any Li associated with calcite dissolution in the experiments with fresh water-based HFF. For the PW experiment, ion exchange reactions were expected to occur due to the high-TDS and circumneutral pH of the influent, which would remove adsorbed Li from exchange sites (e.g., clays and organic). Lack of observable δ^7Li change in the PW experiments is consistent with our previous work showing that negligible Li (< 2%) was extracted from the exchange sites of Marcellus Shale (Phan et al., 2016).

Limited sample volumes precluded analysis of δ^7Li in experiments with diluted produced water with fracturing chemicals, however monitoring changes in Li concentration may provide insight into whether detectable δ^7Li changes due to HFF-shale reactions could occur in

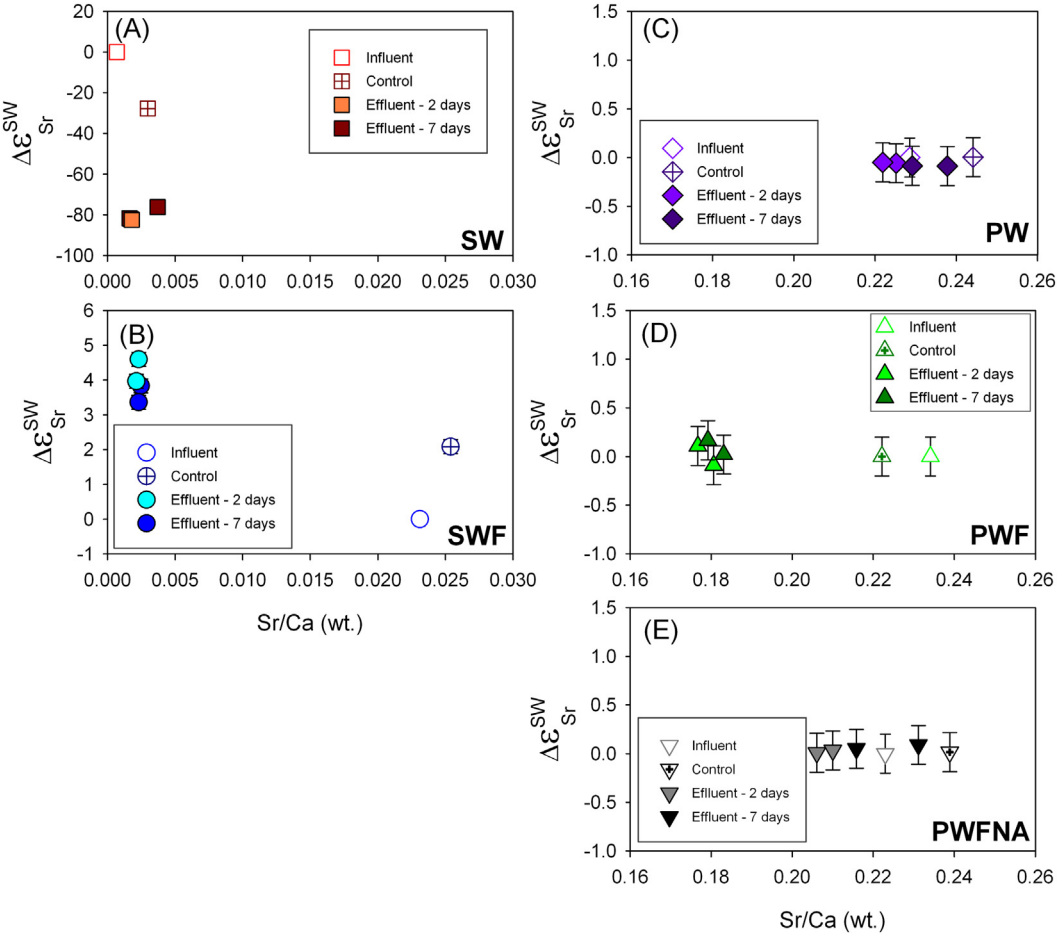

Fig. 4. Variation in $\Delta\varepsilon_{Sr}^{SW}$ ($\Delta\varepsilon_{Sr}^{SW} = \varepsilon_{\text{SW reacted fluid}}^{Sr} - \varepsilon_{\text{SW initial fluid}}^{Sr}$) vs. Sr/Ca of all experiments. Error bars in A and B are within the size of the symbols.

field−collected produced water samples. Higher Li in the effluent of PWF experiments could have been derived from oxidation of pyrite and organic matter from shale. This suggestion is supported by the sequential extraction results (Phan et al., 2016) showing that up to 20% of Li can be associated with sulfides and organic matter in Marcellus Shale. Separate experiments designed to collect ample sample volumes for proper Li isotope processing would be required in the future to characterize whether the changes in Li observed in the PWF experiments are due to carbonate reactions, ion exchange reactions, or oxidation of sulfides and organic matter.

5.2. Application of Sr as an indicator of HFF-shale reactions in core flood experiments

The utility of ε_{Sr}^{SW} as an indicator of HFF-shale reactions depended on the starting Sr concentration and $^{87}Sr/^{86}Sr$ of the experimental influent relative to the potential Sr release and $^{87}Sr/^{86}Sr$ from the shale. In the case of experiments performed with fresh water-based fluids, the starting ε_{Sr}^{SW} notably differed from that coming from the shale, as shown through the clear change in ε_{Sr}^{SW} in the SW and SWF experiments (Table 2). Anticipating that ion exchange and carbonate dissolution are

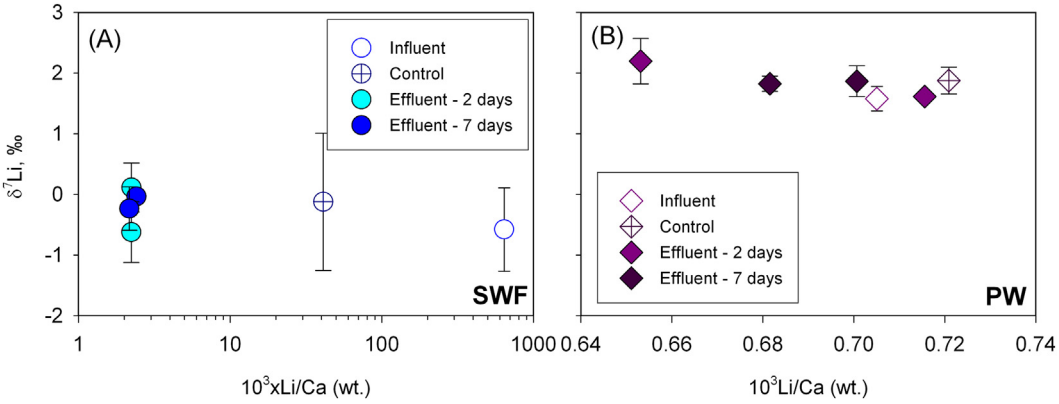

Fig. 5. Variation in δ^7Li vs. 1000*Li/Ca of experiments SWF (A) and experiments PW (B). These figures show that carbonate dissolution and desorption of Li from exchange sites negligibly affect Li concentration and δ^7Li in the reacted fluids.

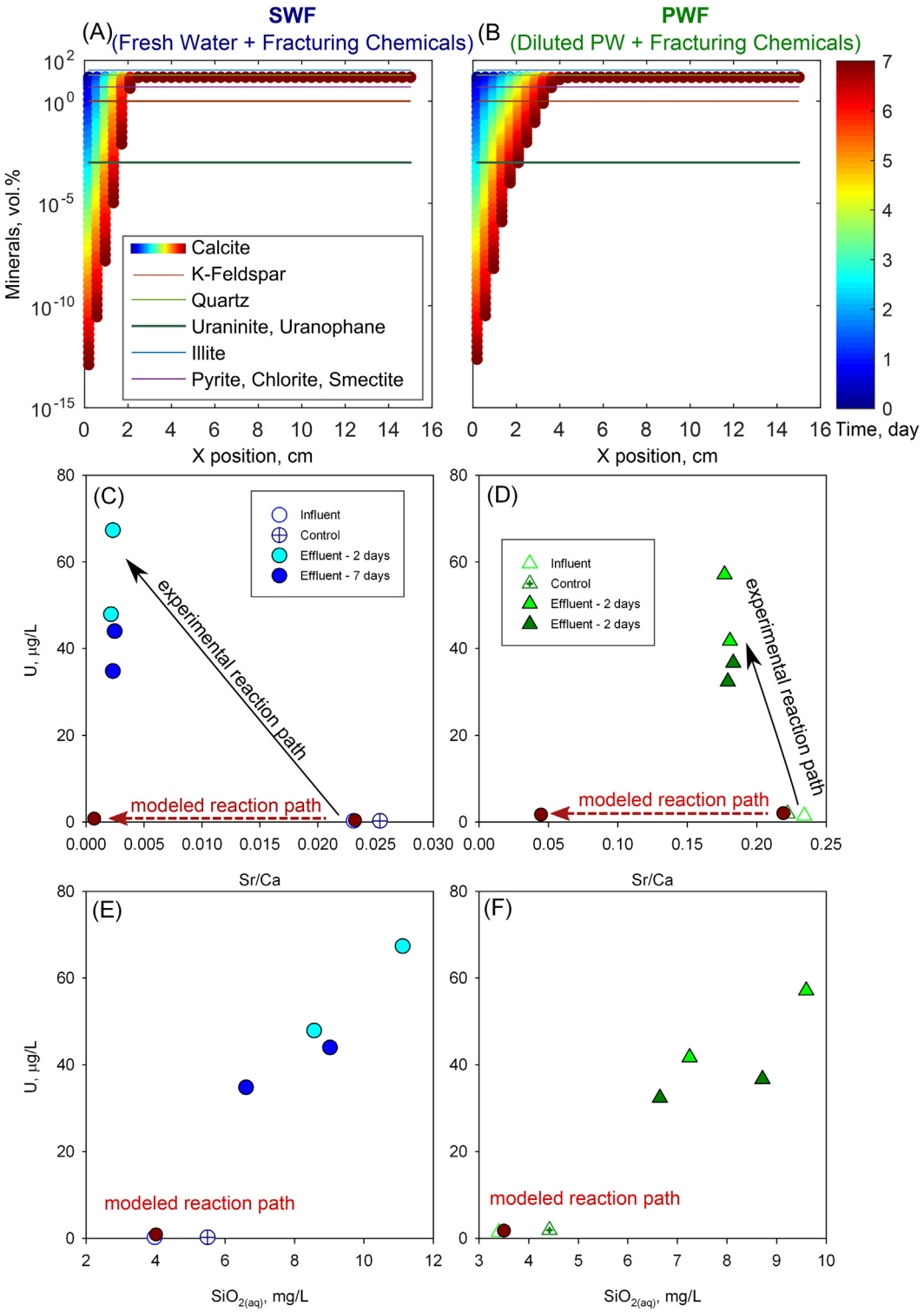

Fig. 6. The 1-D reactive transport models show the temporal change in minerals used in the models (volume %) across the core during the experiments (7 days): freshwater based HFF (A) and produced water based HFF (B). The colored shade on the figure indicate the extent of reaction of calcite throughout the simulation, where the reaction time (day) is indicated by the color of the shade, as shown in the right−hand legend. Models predicted more calcite dissolution (larger area of colored shade) in produced water based HFF than in fresh water based HFF (smaller area of colored shade). Comparison of U vs. Sr/Ca (A, B) and U vs. SiO_2 (C, D) of experimental data and modeled reaction path. U is initially released from calcite dissolution, then subsequently taken up by secondary minerals at later stage as shown by a lower concentration of U in day 7 compared to day 2.

the major contributors towards changes in ε_{Sr}^{SW} due to HFF-shale reactions, the SW experiment without fracturing chemicals or acid is interpreted to result in Sr release due to ion exchange. The SWF experiment containing fracturing fluids with acid is interpreted to result in Sr release due to carbonate mineral dissolution.

It is anticipated that, in field scenarios where waters with different ε_{Sr}^{SW} from the reservoir are applied as the base fluid for HFF, ε_{Sr}^{SW} could be an effective indicator of both ion exchange (per the SW experimental

results) and carbonate (per the SWF experimental results) reactions in the reservoir. The SW experiments exhibited a larger decrease in ε_{Sr}^{SW} (~80 units; Fig. 8) between the influent and effluent, with effluent Sr isotope signatures reflecting those of the exchangeable components of Marcellus Shale ($\varepsilon_{Sr}^{SW} = +9 - +41$; Table 4). This suggests that the increase in Sr in the effluents of the SW experiment was primarily derived from desorption of Sr from shale minerals. Carbonate dissolution releases more radiogenic Sr from carbonate minerals as shown by an increase of ε_{Sr}^{SW} (~4 units) in SWF (Fig. 4B). These ε_{Sr}^{SW} values are within the same range of ε_{Sr}^{SW} values of carbonate components of Marcellus Shale ($\varepsilon_{Sr}^{SW} = -12 - +12$; Table 4) as shown in Fig. 8.

In experiments performed with diluted produced water, the concentration of Sr in the starting fluid was in excess of that anticipated to be released from the shale both in the presence and absence of fracturing chemicals, and with or without acid. The release of Sr from carbonate dissolution does not affect the ε_{Sr}^{SW} in the effluents of PWF (Fig. 8) because the contribution of Sr from carbonate dissolution is negligible in comparison to the Sr concentration in the influent. Extensive secondary barite precipitation was observed in core flood experiments using synthetic produced water (PW, PWF, PWFNA) (Paukert Vankeuren et al., 2017); however, we found that any Sr uptake through secondary mineral precipitation did not affect ε_{Sr}^{SW} in the fluids (within 2SD = 0.02‰; 0.2ε unit) (Fig. 4C, D, E). These results show that incorporation of Sr into barite, if it occurs, does not affect the $^{87}Sr/^{86}Sr$ (i.e. ε_{Sr}^{SW}) ratio of the resulting fluid. While ε_{Sr}^{SW} was an effective indicator for ion exchange and carbonate dissolution reactions in fresh water−based experiments, its utility was diminished for monitoring reactions involving fluids already high in Sr.

The minor concentration contribution of Sr from the shale is obscured by the high Sr concentration in the influent, and therefore the ε_{Sr}^{SW} monitored in experimental effluents from the PW, PWF, and PWFNA experiments is the same value as the influent, within analytical uncertainty. It is anticipated that, in field scenarios where diluted produced water is applied as the HFF base fluid, ε_{Sr}^{SW} will not be an effective indicator of mineral reactions due to HFF-shale interactions.

5.3. Application of U as an indicator of HFF-shale reactions in core flood experiments

The release of U is attributed to acidic dissolution of uranium bearing carbonate minerals (e.g., calcite) and U minerals such as uranium oxides (e.g., uraninite) as suggested in previous studies (Phan et al., 2015, 2018). Concurrent increase in U with a decrease in Sr/Ca (Fig. 6C, D) suggests that U is possibly derived from the dissolution of carbonate minerals. Moreover, the released U in the effluents of experiments performed without HFF (SW, PW) or with HFF but under circumneutral pHs (PWFNA, Table 2) are lower than those performed under acidic conditions.

Even though aqueous silica ($SiO_{2(aq)}$) correlates positively with U measured in the effluents in both SWF and PWF experiments (Fig. 6E, F), the modeling results indicated that quartz and clay minerals did not react and the predicted $SiO_{2(aq)}$ remained constant. Moreover, U is poor in quartz and clays (< 3 mg/kg; Omoniyi et al., 2013; Govindaraju, 1994). Therefore, it is unlikely that high U in the effluents is derived from HFF reacting with quartz and clay minerals in Marcellus Shale.

Concentrations of U in the day 2 and day 7 effluents in both SWF (Fig. 6C) and PWF (Fig. 6D) are due to U release from U-bearing calcite dissolution; as noted previously, U release was not observed from exchangeable sites in Marcellus Shale (Phan et al., 2015). Previous work (Kelly et al., 2006; Sturchio et al., 1998) showed that uranium in both forms, U(VI) and U(IV), was found in the structure of natural calcite. The U/Ca (wt.) ratio in the carbonate fraction of a Marcellus Shale sample ranged from 2.0×10^{-4} to 2.3×10^{-3} (Phan et al., 2015), approximately four orders of magnitude greater than the U/Ca (wt.) ratio in the initial solutions prior to reaction with shale (U/Ca (wt.) of SWF-Influent and PWF-Influent = 9.8×10^{-5} and 7.2×10^{-7}, respectively). With a water-rock (W/R) ratio of 0.01, mass-balance calculations show that it only requires dissolution of < 1% calcite to achieve the U/Ca (wt.) observed in both day 2 and day 7 effluents of SWF and PWF (1.3×10^{-5} to 1.2×10^{-4}). In addition, we observed that the concentrations of U in the effluents of SWF and PWF were similar (Fig. 6C, D), consistent with the similar increase in Ca (~500 mg L^{-1}) in both experiments. Due to this evidence, we suggest that calcite is responsible for releasing U into the effluents of SWF and PWF. This suggestion is also supported by the reactive transport modeling results (Fig. 6A, B). The models showed that uraninite and uranophane dissolution did not occur and there was no notable difference between the predicted concentrations of U in the reacted fluids and the U in the influent (horizontal dashed arrow).

Lower concentrations of U in day 7 effluent relative to day 2 effluent in both experiments coupled with a constant Sr/Ca ratio demonstrated that the released U is likely removed partially from solution via adsorption or incorporation into secondary mineral precipitates, or both. Examples of secondary minerals include iron oxides, gypsum, and barite minerals as documented by high resolution imaging analysis of the reacted core material (Paukert Vankeuren et al., 2017). Similarly, U removal from solution in batch experiments was also observed in a previous study (Marcon et al., 2017).

5.4. Comparison of fluid chemistry changes observed in core flood experiments to produced water from hydraulically fractured Marcellus Shale

Comparison of the core flood experimental results with fluid chemistries of waters produced from hydraulically fractured Marcellus Shale can provide insights on whether geochemical tracers of water-rock reaction are detectable in field samples. One consideration in making this comparison is that the experiments were performed on outcrop core, which provides a perspective on reactions that may occur in deep shale, however may not completely represent geochemical interactions that occur in fracturing operations across the Marcellus Shale. Consideration of the water/rock ratio (W/R) in the core flood experiments versus field conditions is an important factor in extrapolating the experimental results for interpreting field data. Performing our flow−through experiments at a low dosing pump rate (2.4 mL h^{-1}) exposed the rock surface along fractures continuously to fresh fluid at low W/R ratio. Within the experimental cores (170 cm^3), the total measured volume of pore space that could be filled by water was about 6 mL. Assuming a bulk shale density of 2.5 g cm^{-3}, the instantaneous W/R ratio in our experiments was about 0.014 L kg^{-1}, which is comparable to the estimated W/R of 0.01 during hydraulic fracturing (Renock et al., 2016). It is noted that the porosity and surface area of hydraulically fractured shale remain unknown. In our experiments, a rough estimate of fracture surface area per one kg of shale rock ranged from 400 to 600 cm^2 kg^{-1} which is equivalent to 0.023–0.035 mL cm^{-2} (volume of HFF per surface area of fracture) or 1.0–1.5 cm^2 cm^{-3} (surface area per unit volume of rock).

The major cation and anion composition of the experimental fluids are minimally affected by fracture orientation (perpendicular versus parallel), as shown through influent and effluent chemistry comparisons (Fig. 2 this study; Paukert Vankeuren et al., 2017). Experiments of each fluid type with cores fractured parallel and perpendicular to bedding planes cluster in similar regions of the Piper plot. In the spring water-based experiment (SW), the increase in K is observed in the effluent over time (Fig. 3A). The effluent is primarily composed of Ca and K, which is similar to the exchangeable component of Marcellus Shale (pink shade in Fig. 3A). This suggests some cations, such as K and Sr, were released from the exchange sites of clay and organic matter via desorption during the experiment. An increase in Ca relative to Na, K (Fig. 3A), and Cl^- (Fig. 3B) is observed in effluents from experiments performed with both spring water and diluted produced water-based fluids containing HFF with HCl (SWF and PWF, respectively), which is attributed to carbonate dissolution. For comparison to samples from the

Marcellus Shale, major elements such as Na, K, Ca, and Mg in produced water display linear correlations to each other and TDS and increase logarithmically with time after the start of flow back (Haluszczak et al., 2013; Rowan et al., 2015).

Although carbonate dissolution is extensive in the produced water-based experiments (PWF), as demonstrated by X-ray CT imaging of the reacted core material (Paukert Vankeuren et al., 2017), the change in the bulk chemistry is not notable due to initially-high concentrations of Na, Ca, and Cl in the influent. Hence, the released Ca is not high enough to change the relative proportion of Na, Ca, and Cl or Na-Ca-Cl water type in the effluent (Fig. 3B). Occurrence of calcite dissolution in experiments SWF and PWF is supported by a decrease in Sr/Ca weight ratio in both day 2 and day 7 effluents in comparison with the initial fluids (Fig. 4A, B). In experiment SWF, Sr/Ca (wt.) decreased by an order of magnitude from 0.023 (SWF-Influent) to 0.002 (average of day 2 and 7 effluents in the presence of the shale) whereas this change in the Sr/Ca ratio was not observed during the course of the control experiments (Fig. 4; sample SWF0-2 in Table 2). Similarly, Sr/Ca moderately decreased from 0.234 (PWF-Influent) to 0.180 (average of day 2 and 7 effluents in the presence of the shale) in experiments with PWF. A consistently low Sr/Ca value in both day 2 and day 7 effluents of experiments SWF and PWF reflects a continuous supply of Ca from fluid − shale reactions, indicating that calcite dissolution occurred progressively throughout the experiment. For comparison, dissolution of carbonate minerals during hydraulic fracturing possibly results in lower Sr/Ca in Marcellus produced water collected on the first day of flowback than the Sr/Ca in the make-up water (Fig. 8).

Time-series produced water samples showed that δ^7Li and ε_{Sr}^{SW} increased as much as 3‰ (Phan et al., 2016) and 18 ε units (Capo et al., 2014), respectively. These trends were observed in produced water from two types of Marcellus gas wells in Pennsylvania, USA: wells hydraulically fractured by freshwater and reused produced water (Phan et al., 2016). As demonstrated in Fig. 7, Li and Sr display positive linear correlations with TZ^+ ($TZ^+ = Na^+ + 2Mg^{2+} + K^+ + 2Ca^{2+}$ in 10^{-3} equivalents per liter, mEq L^{-1}) in Marcellus make-up water and produced water suggesting that Li and Sr originated from the same source as major elements. However, results from our experiments showed that acidic dissolution of carbonate minerals increased TZ^+ by an order of magnitude in the SWF experiments whereas no changes in Li concentration (Fig. 7A) or δ^7Li values were observed (Fig. 5A). Thus, it is unlikely that the 3 to 6 fold increase in Li concentration observed in produced water from the field over the first 45 days of flowback (Phan et al., 2016) resulted from HFF − shale interactions. Moreover, no significant change in δ^7Li values in experiments exhibiting calcite dissolution also agrees with our previous study that found that hypothetical dissolution of half of the total carbonate minerals in the Marcellus Shale would only increase δ^7Li values in produced water by 0.3‰ as the shale carbonate fraction is poor in Li (Phan et al., 2016).

For the experiments with synthetic produced waters, there were no noticeable changes in TZ^+ in any experiments (PW, PWF, and PWFNA). There was also no change in δ^7Li values (analyzed for PW only; Fig. 5B), Sr (Fig. 7B), and ε_{Sr}^{SW} (Fig. 4C, D, E). In contrast, TZ^+ of produced water from a gas well that was hydraulically fractured using diluted produced water as make-up water increased 1.3 times within the first week of flow back (Well A, Table 1 in Rowan et al., 2015). The δ^7Li and ε_{Sr}^{SW} values in produced water from this same well also increased by 1‰ (well 9; Phan et al., 2016) and 15 units (well GR; Chapman et al., 2012) respectively, within the first 20 days. In addition, ε_{Sr}^{SW} of carbonate components of the Marcellus Shale ranged from −12 to 12 units, which is lower than ε_{Sr}^{SW} of the make − up water (ε_{Sr}^{SW} = 13; Fig. 8) of a well in Greene County, PA. If the chemical composition of day 1 flowback water (water produced on the first day well production) were predominantly controlled by the dissolution of carbonate minerals, the ε_{Sr}^{SW} would decrease to a value that is lower than the make-up water

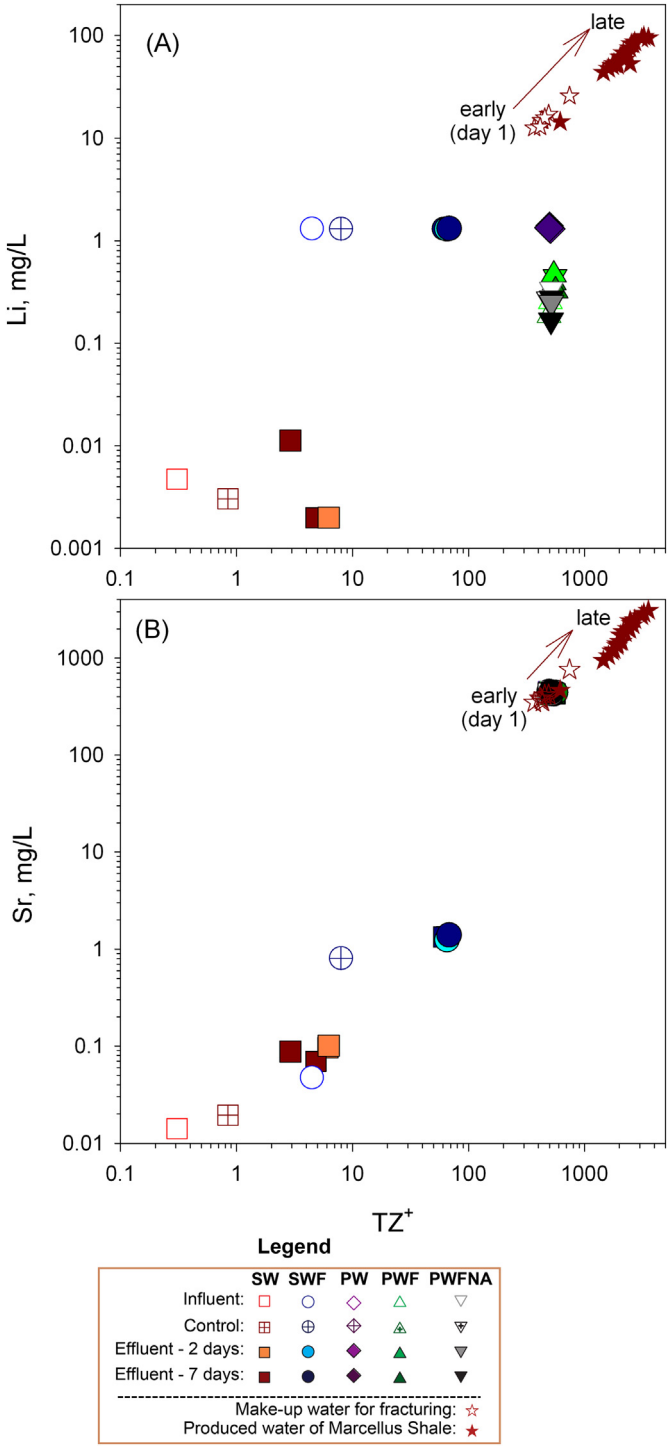

Fig. 7. Variation in Li (A) and Sr (B) vs. total cation charge TZ^+ which is defined as: $TZ^+ = Na^+ + 2Mg^{2+} + K^+ + 2Ca^{2+}$ as milliequivalent per liter, mEq L^{-1}. Marcellus produced water and make-up water (Hayes, 2009; Rowan et al., 2015) are shown for comparison.

(ε_{Sr}^{SW} = 13). However, the ε_{Sr}^{SW} of day 1 flowback water from this well was 26 units, greater than the ε_{Sr}^{SW} of the make-up water (Chapman et al., 2012). The changes in TZ^+, δ^7Li, and ε_{Sr}^{SW} in the hydraulically fractured well during the flowback period contrast with a lack of change in the same parameters in the three PW core flooding experiments. This suggests that water-rock interaction processes, particularly

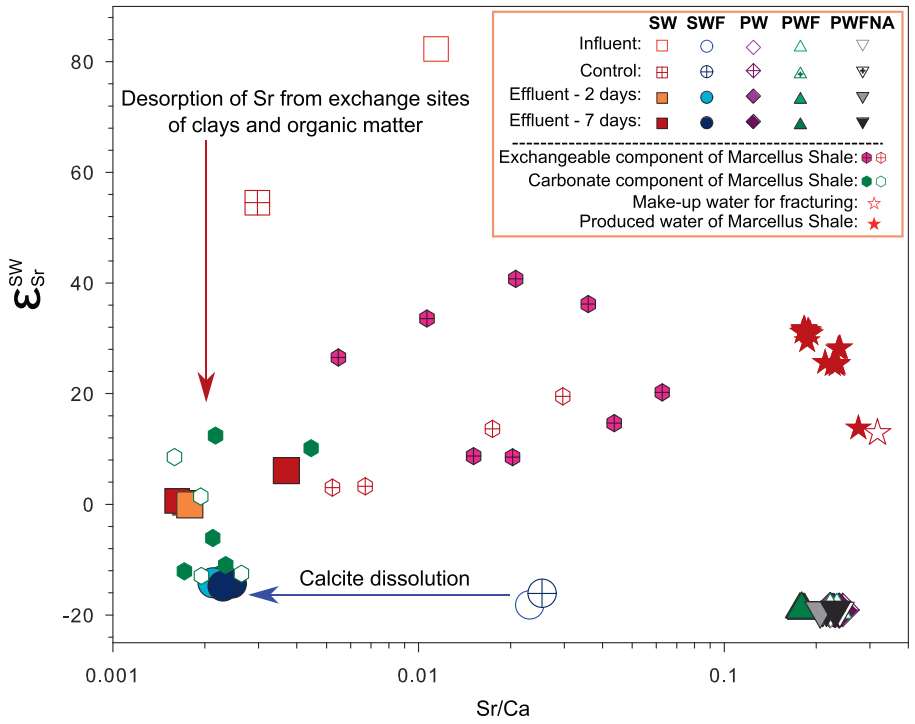

Fig. 8. Comparison of ε_{Sr}^{SW} in the effluents of the experiments with ε_{Sr}^{SW} in extracted components of Marcellus Shale and Marcellus Shale produced waters (filled symbols). Additional data of the extracted components are from a previous study (open symbols; Stewart et al., 2015) and produced water data of a Marcellus well in Greene County, PA, USA (Chapman et al., 2012; Capo et al., 2014) are shown for comparison.

the dissolution and precipitation of carbonate minerals, are neither the primary influence on the composition of day 1 flowback water nor the source of the continued increase in the salinity observed in produced water from the field.

Additionally, no changes in Cl/Br and Na/Br ratios were observed in any of the core flooding experiments (Table 2) (though the concentrations of Br in the effluents of experiments with fresh spring water (SW) were lower than the method detection limit, thus Cl/Br and Na/Br ratios are not calculated for that experiment). In contrast, time − series produced water samples shifted towards Br–enrichment (i.e. lowering Cl/Br and Na/Br ratios) following the seawater evaporation trend (Rowan et al., 2015) regardless of whether gas wells were fractured by freshwater or reused produced water. Thus, no change in Cl/Br and Na/Br ratios observed in laboratory experiments imply that water-rock interactions, such as halite dissolution, do not likely contribute to temporal salinity evolution of produced waters from hydraulically − -fractured shales. Otherwise, the Cl/Br and Na/Br ratios should have increased in the experimental fluids. The lack of halite dissolution is further supported by results from sequential extractions of shale rocks of both Oatka Creek and Union Springs members of Marcellus Shale (Table 4), which showed that, based on Na extracted in water soluble fraction, halite makes up < 0.2% of the Marcellus Shale.

In summary, the variations in the concentration and isotopes of Li and Sr vs. TZ^+ from the experiments reported here do not agree with the temporal positive correlations between Li and Sr vs. TZ^+ observed in produced water from the field. In addition, changes in δ^7Li and ε_{Sr}^{SW} in our experiments do not replicate the increasing magnitude of δ^7Li and ε_{Sr}^{SW} in real produced water. If we can extrapolate from our experimental results on the outcrop material of Marcellus to field observations across the entire play, the experimental results suggest that water-rock reactions do not exert a strong influence on the evolution of Marcellus Shale produced water chemistry. Instead, it is likely that mixing or diffusion of formation water into injected fracturing fluids is the primary driver of produced water chemistry. Future experimental work involving shale cores and fluids from sections of the formation undergoing fracturing and production will further test this hypothesis.

5.5. Potential for application of U as an indicator of HFF-shale reactions in hydraulically fractured Marcellus Shale

The experimental results in this study demonstrated that the highest concentration of U occurred in the day 2 effluent samples of the SWF and PWF experiments. That acidic influents in both experiments resulted in a release of U (up to 67 μg L^{-1}) concurrently with Ca (Fig. 6C, D) due to calcite dissolution is also supported by the reactive transport modeling results. Lower concentrations of U were released in experiments performed with HFF at circumneutral pHs that exhibited limited calcite dissolution (SW, PW, and PWFNA, Table 2). An initial release of U due to carbonate mineral dissolution is supported by our previous study showed that U in Marcellus produced water was at its highest concentration on the first day of flow back, decreased to < 0.1 μg L^{-1} (reporting limit) after 30 days, then remained constant over the duration (813 days) of sampling (Phan et al., 2015). Sequential extractions also reinforced the idea of carbonates as a source of U because substantial U (up to 20% of U in bulk rock samples from a drilled core) was extracted in the acetic acid soluble fraction of Marcellus Shale (Phan et al., 2015), which is primarily derived from carbonate minerals.

Aqueous silica ($SiO_{2(aq)}$) was found to positively correlate with U in both SWF and PWF experiments (Fig. 4C, D). Simultaneous release of Al and $SiO_{2(aq)}$ resulting from HFF and shale interactions in these two experiments (Table 2) suggests that dissolution of clays could have occurred to some degree, as observed in a previous study of HFF and shale interactions in batch experiments (Marcon et al., 2017). In contrast, our models showed that aluminosilicate minerals would not dissolve, and silica concentration would remain constant (Fig. 4). Thus, the release of $SiO_{2(aq)}$ and Al is likely due to the contribution of

colloidal clays that went through the 0.45 μm membrane during filtration of experimental samples; however, this hypothesis requires further study to confirm. Even so, we do not expect clays to be the primary source of U because its concentration in clays is poor (< 3 mg/kg; Omoniyi et al., 2013) and kinetic dissolution rates of clays are much lower than calcite under acidic conditions in these experiments. For comparison, U in carbonate of the Marcellus Shale was measured as high as 76 mg/kg of carbonate (Phan et al., 2015).

Results from our reactive transport model also show that uranophane dissolution would not occur. Hence, uranophane, a secondary mineral containing both U and Si, is likely not the cause for simultaneous release of U and $SiO_{2(aq)}$ due both to kinetic limitations and the lack of observed uranophane in Marcellus Shale cores (Leventhal, 1987). Uranophane is commonly observed as a weathering product of uraninite under oxidizing conditions (Pearcy et al., 1994), thus it might be present in our outcrop samples although its presence in Marcellus Shale has not been reported to date. Although uraninite has been identified in Marcellus Shale samples (Fortson, 2012), the dissolution of uraninite is also kinetically limited, especially under anoxic conditions in the subsurface as demonstrated in the modeling results. Therefore, we conclude that dissolution of carbonate minerals is the main cause of U release observed in the experiments conducted under acidic conditions.

Based on the experimental results from this study and observations from our prior studies, acidic dissolution of U − containing calcite is anticipated to control the U pulse observed in produced waters obtained during early flowback. HCl is among the top four commonly used chemical substances during hydraulic fracturing (Konschnik and Dayalu, 2016; U.S. Envrionmental Protection Agency, 2015) to dissolve cement and reactive minerals such as calcite, in order to provide a pathway for fracturing fluids to break the rock. Calcite dissolution could continue to take place during the well shut-in period although the pH of the earliest produced water was circumneutral (Hayes, 2009). Regarding the temporal decreasing trend of U in Marcellus produced water, we propose two hypotheses that could explain the decrease in U over time. If redox conditions in the subsurface become anoxic over time, reductive precipitation of uranium as insoluble U(IV) (e.g., as uraninite; Wall and Krumholz, 2006) would decrease the soluble U in produced water. The decreasing U trend over time also could be explained by primary mixing between fluid with high U (resulting from shale − fracturing fluid reactions) and pre − existing formation water with negligible U.

6. Conclusions

This study used analysis of fluids from shale-HFF core flood experiments to evaluate the application of solution-phase geochemical tracers as indicators of water-rock interactions that occur during hydraulic fracturing. We also characterized three components of shale (water soluble, exchangeable, and carbonate fractions) which were sequentially − extracted as part of a separate study (Phan et al., 2015) and analyzed as part of this study to compare with the reacted fluids from the core flood experiments. This study aimed to determine if Sr and Li isotopes and U concentration could be used to identify reactions between HFF and major minerals in shale.

Overall, the experimental results show that HFF-shale reactions without the presence of formation water exhibited differing trends in Li and Sr isotopic signatures and TDS from those observed in Marcellus Shale produced waters. Additional experiments on drill cuttings and fresh core materials covering a wide range of mineralogical compositions found in Marcellus Shale are required to thoroughly understand water − rock interactions during hydraulic fracturing of this formation. However, these results support previous observations that produced water composition is primarily the result of the mixing of the injected fluid with pre-existing formation water (Capo et al., 2014; Haluszczak et al., 2013; Phan et al., 2016; Rowan et al., 2015; Stewart et al., 2015).

The experimental results involving U geochemistry suggest that calcite dissolution due to reaction with acidic fracturing fluids could explain the pulse of U observed in produced waters returned on the first day of flowback. However, the subsequent decline of U in both the experimental fluids and produced waters after the early increase in concentration demonstrates that U-controlling reactions (precipitation, redox, and/or sorption) or fluid mixing between reacted fluids and existing formation fluids occurs. This relationship is based on the observations from the core flood experimental study and will require additional experimentation in the laboratory and field for verification. Future investigation on the temporal evolution of redox conditions in the subsurface will also be crucial for understanding the mobility of redox sensitive elements (e.g., U), and the potential effects of microbial activities and secondary precipitation reactions on fracture permeability and shale matrix porosity.

Water − rock interactions are expected to influence the geochemical behavior of various components in Marcellus produced water such as Ba (Phan et al., 2015; Renock et al., 2016) that can result in low solubility barite formation, and low molecular weight organic acids (Akob et al., 2015) that can influence mineral dissolution and precipitation reactions in fractured shale and thus affect gas production from unconventional reservoirs. Although these water − rock reactions may not be detected solely through monitoring major ions of produced water, future development of tracers for characterizing mineral reactions in the reservoir can lead to improved hydraulic fracturing design and more efficient gas production from unconventional shales.

Acknowledgements

We thank Dr. C. Özgen Karacan for handling the manuscript and two anonymous reviewers and for their insightful comments that helped us greatly improved this manuscript. This study was supported by the U.S. Department of Energy, Office of Fossil Energy, as the National Energy Technology Laboratory's ongoing research. We thank Dustin Crandall (NETL), Johnathan Moore (AECOM/NETL), and Karl Jarvis (AECOM/NETL) for help with the flow–through experimental setup, Daniel Bain for technical support with ICP-MS analysis at the University of Pittsburgh, and Daniel Soeder (NETL, retired) for providing the Marcellus Shale outcrop samples. Brian Stewart and Rosemary Capo (University of Pittsburgh) are thanked for providing clean lab space for sample preparation for isotopic analysis. This research was supported in part by appointments to the National Energy Technology Laboratory Research Participation Program, sponsored by the U.S. Department of Energy and administered by the Oak Ridge Institute for Science and Education (TTP, ANPV).

Disclaimers

Any opinions, findings, conclusions, or recommendations expressed herein are those of the authors and do not necessarily reflect the views of the sponsors. Reference in this paper to any specific commercial product, process, or service is to facilitate understanding and does not imply endorsement by the United States Department of Energy.

References

Akob, D.M., Cozzarelli, I.M., Dunlap, D.S., Rowan, E.L., Lorah, M.M., 2015. Organic and inorganic composition and microbiology of produced waters from Pennsylvania shale gas wells. Appl. Geochem. 60, 116–125.

Balashov, V.N., Engelder, T., Gu, X., Fantle, M.S., Brantley, S.L., 2015. A model describing flowback chemistry changes with time after Marcellus Shale hydraulic fracturing. AAPG Bull. 99 (1), 143–154.

Bethke, C., 2008. Geochemical and Biogeochemical Reaction Modeling. Cambridge University Press Cambridge.

Brantley, S.L., 2008. Kinetics of Mineral Dissolution, Kinetics of Water-Rock Interaction. Springer, pp. 151–210.

Brantley, S.L., Yoxtheimer, D., Arjmand, S., Grieve, P., Vidic, R., Pollak, J., Llewellyn, G.T., Abad, J., Simon, C., 2014. Water resource impacts during unconventional shale

gas development: the Pennsylvania experience. Int. J. Coal Geol. 126, 140–156.
Bryant, C.J., McCulloch, M.T., Bennett, V.C., 2003. Impact of matrix effects on the accurate measurement of Li isotope ratios by inductively coupled plasma mass spectrometry (MC-ICP-MS) under "cold" plasma conditions. J. Anal. At. Spectrom. 18 (7), 734–737.
Capo, R.C., Stewart, B.W., Rowan, E.L., Kolesar Kohl, C.A., Wall, A.J., Chapman, E.C., Hammack, R.W., Schroeder, K.T., 2014. The strontium isotopic evolution of Marcellus formation produced waters, southwestern Pennsylvania. Int. J. Coal Geol. 126, 57–63.
Casas, I., Bruno, J., Cera, E., Finch, R., Ewing, R., 1994. Kinetic and thermodynamic studies of uranium minerals. In: Assessment of the Long-Term Evolution of Spent Nuclear Fuel. Swedish Nuclear Fuel and Waste Management Co..
Chapman, E.C., Capo, R.C., Stewart, B.W., Kirby, C.S., Hammack, R.W., Schroeder, K.T., Edenborn, H.M., 2012. Geochemical and strontium isotope characterization of produced waters from Marcellus Shale natural gas extraction. Environ. Sci. Technol. 46, 3545–3553.
Cipolla, C.L., Lolon, E.P., Erdle, J.C., Rubin, B., 2010. Reservoir modeling in shale-gas reservoirs. SPE Reserv. Eval. Eng. 13, 638–653.
Dieterich, M., Kutchko, B., Goodman, A., 2016. Characterization of Marcellus Shale and Huntersville Chert before and after exposure to hydraulic fracturing fluid via feature relocation using field-emission scanning electron microscopy. Fuel 182, 227–235.
Dong, W., Brooks, S.C., 2006. Determination of the formation constants of ternary complexes of uranyl and carbonate with alkaline earth metals (Mg^{2+}, Ca^{2+}, Sr^{2+}, and Ba^{2+}) using anion exchange method. Environ. Sci. Technol. 40, 4689–4695.
Fortson, L., 2012. Geochemical and Spatial Investigation of Uranium in the Marcellus Shale. State University of New York at Buffalo.
Gautier, J.-M., Oelkers, E.H., Schott, J., 1994. Experimental study of K-feldspar dissolution rates as a function of chemical affinity at 150 C and pH 9. Geochim. Cosmochim. Acta 58, 4549–4560.
Govindaraju, K., 1994. Compilation of working values and sample description for 383 geostandards. Geostand. Newslett. 18, 1–158.
Haluszczak, L.O., Rose, A.W., Kump, L.R., 2013. Geochemical evaluation of flowback brine from Marcellus gas wells in Pennsylvania, USA. Appl. Geochem. 28, 55–61.
Harrison, A.L., Jew, A.D., Dustin, M.K., Thomas, D.L., Joe-Wong, C.M., Bargar, J.R., Johnson, N., Brown Jr, G.E., Maher, K., 2017. Element release and reaction-induced porosity alteration during shale-hydraulic fracturing fluid interactions. Appl. Geochem. 82, 47–62.
Hayes, T., 2009. Sampling and analysis of water streams associated with the development of marcellus shale gas. In: Report by the Gas Technology Institute. Marcellus Shale Coalition, Des Plaines, IL.
Heidari, P., Li, L., Jin, L., Williams, J.Z., Brantley, S.L., 2017. A reactive transport model for Marcellus shale weathering. Geochim. Cosmochim. Acta 217, 421–440.
Hellevang, H., Pham, V.T., Aagaard, P., 2013. Kinetic modelling of CO_2–water–rock interactions. Int. J. Greenhouse Gas Control 15, 3–15.
Hosterman, J.W., Whitlow, S.I., 1983. Clay Mineralogy of Devonian Shales in the Appalachian Basin; Geological Survey Professional Paper 1298. Washington, D.C, United States Geological Survey.
Hsi, C.-k.D., Langmuir, D., 1985. Adsorption of uranyl onto ferric oxyhydroxides: application of the surface complexation site-binding model. Geochim. Cosmochim. Acta 49, 1931–1941.
Jew, A.D., et al., 2017. Impact of organics and carbonates on the oxidation and precipitation of iron during hydraulic fracturing of shale. Energy Fuel 31 (4), 3643–3658.
Jin, L., et al., 2013. Evolution of porosity and geochemistry in Marcellus Formation black shale during weathering. Chem. Geol. 356, 50–63.
Kelly, S.D., Rasbury, E.T., Chattopadhyay, S., Kropf, A.J., Kemner, K.M., 2006. Evidence of a stable uranyl site in ancient organic-rich calcite. Environ. Sci. Technol. 40, 2262–2268.
Kolesar Kohl, C.A., Capo, R.C., Stewart, B.W., Wall, A.J., Schroeder, K.T., Hammack, R.W., Guthrie, G.D., 2014. Strontium isotopes test long-term zonal isolation of injected and Marcellus formation water after hydraulic fracturing. Environ. Sci. Technol. 48, 9867–9873.
Konschnik, K., Dayalu, A., 2016. Hydraulic fracturing chemicals reporting: analysis of available data and recommendations for policymakers. Energ Policy 88, 504–514.
Langmuir, D., 1978. Uranium solution-mineral equilibria at low temperatures with applications to sedimentary ore deposits. Geochim. Cosmochim. Acta 42, 547–569.
Lasaga, A.C., 1984. Chemical kinetics of water-rock interactions. J. Geophys. Res. Solid Earth 89, 4009–4025.
Lee, D.S., Herman, J.D., Elsworth, D., Kim, H.T., Lee, H.S., 2011. A critical evaluation of unconventional gas recovery from the marcellus shale, northeastern United States. KSCE J. Civ. Eng. 15, 679–687.
Leventhal, J.S., 1987. Carbon and sulfur relationships in Devonian shales from the Appalachian Basin as an indicator of environment of deposition. Am. J. Sci. 287, 33–49.
Lin, J., Liu, Y., Hu, Z., Yang, L., Chen, K., Chen, H., Zong, K., Gao, S., 2016. Accurate determination of lithium isotope ratios by MC-ICP-MS without strict matrix-matching by using a novel washing method. J. Anal. At. Spectrom. 31, 390–397.
Macpherson, G.L., Capo, R.C., Stewart, B.W., Phan, T.T., Schroeder, K., Hammack, R.W., 2014. Temperature-dependent Li isotope ratios in Appalachian Plateau and Gulf Coast Sedimentary Basin saline water. Geofluids 14, 419–429.
Marcon, V., Joseph, C., Carter, K.E., Hedges, S.W., Lopano, C.L., Guthrie, G.D., Hakala, J.A., 2017. Experimental insights into geochemical changes in hydraulically fractured Marcellus shale. Appl. Geochem. 76, 36–50.
Milici, R.C., Swezey, C., 2006. Assessment of Appalachian Basin Oil and Gas Resources: Devonian Shale-Middle and Upper Paleozoic Total Petroleum System. US Department of the Interior, US Geological Survey.
Neymark, L.A., Premo, W.R., Mel'nikov, N.N., Emsbo, P., 2014. Precise determination of $\delta^{88}Sr$ in rocks, minerals, and waters by double-spike TIMS: a powerful tool in the study of geological, hydrological and biological processes. J. Anal. At. Spectrom. 29, 65–75.
Noack, C.W., Jain, J.C., Stegmeier, J., Hakala, J.A., Karamalidis, A.K., 2015. Rare earth element geochemistry of outcrop and core samples from the Marcellus shale. Geochem. Trans. 16, 6.
Omoniyi, I.M., Oludare, S.M.B., Oluwaseyi, O.M., 2013. Determination of Radionuclides and Elemental Composition of Clay Soils by Gamma- and X-ray Spectrometry. 2. SpringerPlus, pp. 74.
Palandri, J.L., Kharaka, Y.K., 2004. A Compilation of Rate Parameters of Water-Mineral Interaction Kinetics for Application to Geochemical Modeling. DTIC Document.
Paukert Vankeuren, A.N., Hakala, J.A., Jarvis, K., Moore, J.E., 2017. Mineral reactions in Shale Gas Reservoirs: Barite scale formation from reusing produced water as hydraulic fracturing fluid. Environ. Sci. Technol. 51, 9391–9402.
Pearce, J.K., Turner, L., Pandey, D., 2018. Experimental and predicted geochemical shale-water reactions: Roseneath and Murteree shales of the Cooper Basin. Int. J. Coal Geol. 187, 30–44.
Pearcy, E.C., Prikryl, J.D., Murphy, W.M., Leslie, B.W., 1994. Alteration of uraninite from the Nopal I deposit, Penã Blanca District, Chihuahua, Mexico, compared to degradation of spent nuclear fuel in the proposed U.S. high-level nuclear waste repository at Yucca Mountain, Nevada. Appl. Geochem. 9, 713–732.
Petsch, S.T., Berner, R.A., Eglinton, T.I., 2000. A field study of the chemical weathering of ancient sedimentary organic matter. Org. Geochem. 31 (5), 475–487.
Phan, T.T., Capo, R.C., Stewart, B.W., Graney, J.R., Johnson, J.D., Sharma, S., Toro, J., 2015. Trace metal distribution and mobility in drill cuttings and produced waters from Marcellus Shale gas extraction: uranium, arsenic, barium. Appl. Geochem. 60, 89–103.
Phan, T.T., Capo, R.C., Stewart, B.W., Macpherson, G., Rowan, E.L., Hammack, R.W., 2016. Factors controlling Li concentration and isotopic composition in formation waters and host rocks of Marcellus Shale, Appalachian Basin. Chem. Geol. 420, 162–179.
Phan, T.T., Gardiner, J.B., Capo, R.C., Stewart, B.W., 2018. Geochemical and multi-isotopic ($^{87}Sr/^{86}Sr$, $^{143}Nd/^{144}Nd$, $^{238}U/^{235}U$) perspectives of sediment sources, depositional conditions, and diagenesis of the Marcellus Shale, Appalachian Basin, USA. Geochim. Cosmochim. Acta 222, 187–211.
Piper, A.M., 1944. A Graphic Procedure in the Geochemical Interpretation of Water-Analyses Eos, Transactions. Vol. 25. American Geophysical Union, pp. 914–928.
Pokrovsky, O.S., Golubev, S.V., Schott, J., Castillo, A., 2009. Calcite, dolomite and magnesite dissolution kinetics in aqueous solutions at acid to circumneutral pH, 25 to 150 C and 1 to 55 atm pCO_2: new constraints on CO_2 sequestration in sedimentary basins. Chem. Geol. 265, 20–32.
Renock, D., Landis, J.D., Sharma, M., 2016. Reductive weathering of black shale and release of barium during hydraulic fracturing. Appl. Geochem. 65, 73–86.
Rimstidt, J.D., Barnes, H., 1980. The kinetics of silica-water reactions. Geochim. Cosmochim. Acta 44, 1683–1699.
Rowan, E.L., Engle, M.A., Kraemer, T.F., Schroeder, K.T., Hammack, R.W., Doughten, M.W., 2015. Geochemical and isotopic evolution of water produced from Middle Devonian Marcellus Shale gas wells, Appalachian Basin, Pennsylvania. AAPG Bull. 99, 181–206.
Soeder, D.J., Sharma, S., Pekney, N., Hopkinson, L., Dilmore, R., Kutchko, B., Stewart, B., Carter, K., Hakala, A., Capo, R., 2014. An approach for assessing engineering risk from shale gas wells in the United States. Int. J. Coal Geol. 126, 4–19.
Stewart, B.W., Chapman, E.C., Capo, R.C., Johnson, J.D., Graney, J.R., Kirby, C.S., Schroeder, K.T., 2015. Origin of brines, salts and carbonate from shales of the Marcellus Formation: evidence from geochemical and Sr isotope study of sequentially extracted fluids. Appl. Geochem. 60, 77–88.
Sturchio, N., Antonio, M., Soderholm, L., Sutton, S., Brannon, J., 1998. Tetravalent uranium in calcite. Science 281, 971–973.
Suzuki, Y., Kelly, S.D., Kemner, K.M., Banfield, J.F., 2002. Radionuclide contamination: nanometre-size products of uranium bioreduction. Nature 419, 134.
Sylwester, E.R., Hudson, E.A., Allen, P.G., 2000. The structure of uranium (VI) sorption complexes on silica, alumina, and montmorillonite. Geochim. Cosmochim. Acta 64, 2431–2438.
Tasker, T.L., Piotrowski, P.K., Dorman, F.L., Burgos, W.D., 2016. Metal associations in Marcellus shale and fate of synthetic hydraulic fracturing fluids reacted at high pressure and temperature. Environ. Eng. Sci. 33, 753–765.
Torrero, M., Baraj, E., De Pablo, J., Gimenez, J., Casas, I., 1997. Kinetics of corrosion and dissolution of uranium dioxide as a function of pH. In. J. Chem. Kinet. 29, 261–267.
U.S. Envrionmental Protection Agency, 2015. Analysis of Hydraulic Fracturing Fluid Data from the FracFocus Chemical Disclosure Registry 1.0. Office of Research and Development, Washington, DC (EPA/601/R-14/003).
Ulrich, K.-U., Ilton, E.S., Veeramani, H., Sharp, J.O., Bernier-Latmani, R., Schofield, E.J., Bargar, J.R., Giammar, D.E., 2009. Comparative dissolution kinetics of biogenic and chemogenic uraninite under oxidizing conditions in the presence of carbonate. Geochim. Cosmochim. Acta 73, 6065–6083.
Wall, J.D., Krumholz, L.R., 2006. Uranium reduction. Annu. Rev. Microbiol. 60, 149–166.
Wall, A.J., Capo, R.C., Stewart, B.W., Phan, T.T., Jain, J.C., Hakala, J.A., Guthrie, G.D., 2013. High throughput method for Sr extraction from variable matrix waters and $^{87}Sr/^{86}Sr$ isotope analysis by MC-ICP-MS. J. Anal. At. Spectrom. 28, 1338–1344.

Wang, G., Carr, T.R., 2012. Methodology of organic-rich shale lithofacies identification and prediction: a case study from Marcellus Shale in the Appalachian basin. Comput. Geosci. 49, 151–163.
Wendt, A.K., Arthur, M.A., Slingerland, R., Kohl, D., Bracht, R., Engelder, T., 2015. Geochemistry and depositional history of the Union Springs Member, Marcellus Formation in central Pennsylvania. Interpretation 3, SV17–SV33.
Wilke, F.D., Vieth-Hillebrand, A., Naumann, R., Erzinger, J., Horsfield, B., 2015. Induced mobility of inorganic and organic solutes from black shales using water extraction: implications for shale gas exploitation. Appl. Geochem. 63, 158–168.
Wilkins, S., Mount, V., Mahon, K., Perry, A., Koenig, J., 2014. Characterization and development of subsurface fractures observed in the Marcellus Formation, Appalachian Plateau, north-central Pennsylvania. AAPG Bull. 98, 2301–2345.
Xu, T., Sonnenthal, E., Spycher, N., Pruess, K., 2006. TOUGHREACT - A simulation program for non-isothermal multiphase reactive geochemical transport in variably saturated geologic media: Applications to geothermal injectivity and CO_2 geological sequestration. Comput. Geosci. 32, 145–165.